

# Going Further: Flatness at the Rescue of Early Stopping for Adversarial Example Transferability

Martin Gubri\*<sup>1</sup>

Maxime Cordy<sup>2</sup>

Yves Le Traon<sup>2</sup>

<sup>1</sup>Parameter Lab, Tübingen, Germany

<sup>2</sup>University of Luxembourg, Luxembourg, Luxembourg

## Abstract

Transferability is the property of adversarial examples to be misclassified by other models than the surrogate model for which they were crafted. Previous research has shown that early stopping the training of the surrogate model substantially increases transferability. A common hypothesis to explain this is that deep neural networks (DNNs) first learn robust features, which are more generic, thus a better surrogate. Then, at later epochs, DNNs learn non-robust features, which are more brittle, hence worst surrogate. First, we tend to refute this hypothesis, using transferability as a proxy for representation similarity. We then establish links between transferability and the exploration of the loss landscape in parameter space, focusing on sharpness, which is affected by early stopping. This leads us to evaluate surrogate models trained with seven minimizers that minimize both loss value and loss sharpness. Among them, SAM consistently outperforms early stopping by up to 28.8 percentage points. We discover that the strong SAM regularization from large flat neighborhoods tightly links to transferability. Finally, the best sharpness-aware minimizers prove competitive with other training methods and complement existing transferability techniques.

## 1 INTRODUCTION

State-of-the-art Deep Neural Networks (DNNs) are vulnerable to imperceptible worst-case inputs perturbations, so-called adversarial examples [Biggio et al., 2013, Szegedy et al., 2013]. These perturbations are not simple flukes of specific representations because some are simultaneously

\*Work conducted during the author’s PhD at the University of Luxembourg.

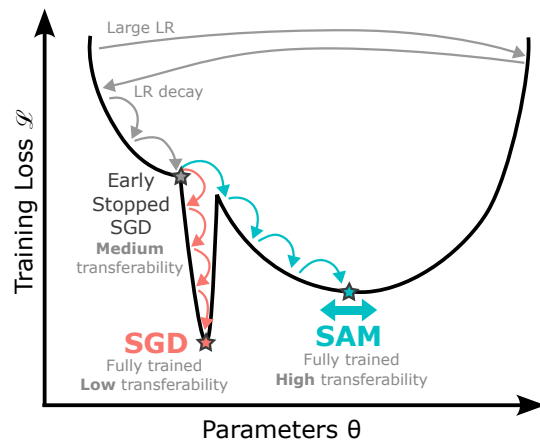


Figure 1: Illustration of the loss landscape, showing the training of surrogate models to craft transferable adversarial examples. Before the learning rate decays, training tends to “cross the valley” with plateauing transferability. A few iterations after the decay of the learning rate, early stopped SGD achieves its best transferability (gray). In the following epochs, SGD falls progressively into deep, sharp holes in the parameter space with poor transferability (red). I-SAM (blue) avoids these holes by minimizing the maximum loss around an unusually large neighborhood (thick blue arrow).

adversarial against several independently trained models with distinct architectures [Goodfellow et al., 2014]. This observation leads to the discovery of the *transferability* of adversarial examples, i.e., an adversarial example against a model is likely to be adversarial against another model. This phenomenon is not well understood but has practical implications. Indeed, practitioners cannot rely on security by obscurity. Attackers can apply white-box attacks to their *surrogate model* to fool an unknown *target model*. These types of attack are called transfer-based back-box attacks. They do not require *any* query access to the model to craft adversarial examples. Crafting highly transferable adversarial examples for distinct architectures is still an open problem

[Naseer et al., 2022] and an active area of research [Benz et al., 2021, Dong et al., 2018, Gubri et al., 2022a,b, Li et al., 2018, Lin et al., 2019, Springer et al., 2021, Wu et al., 2020, Xie et al., 2019, Zhao et al., 2022]. Understanding the underlining characteristics that drive transferability provides insights into how DNNs learn generic representations.

Despite strong interest in transferability, little attention has been paid to how to train better surrogate models. The most commonly used method is arguably *early stopping* [Benz et al., 2021, Zhang et al., 2021, Nitin, 2021] – which is originally a practice to improve natural generalization. The commonly accepted hypothesis to explain why early stopping improves transferability is that an early stopped DNN is composed of more robust features, whereas the fully trained counterpart has more brittle non-robust features [Benz et al., 2021, Zhang et al., 2021, Nitin, 2021].

In this paper, we invalidate this hypothesis empirically and uncover other explanations behind the effectiveness of early stopping, and more generally on how to achieve better surrogate training. We observe in Section 3 that early stopping also improves transferability from and to models composed of *non-robust* features. We propose an alternative hypothesis centered on the dynamics of loss surface exploration, with a focus on sharpness. Section 4 motivates this approach, highlighting that transferability peaks when the loss sharpness in the weight space drops. Section 5 shows that seven optimizers significantly increase the transferability of a surrogate model by minimizing its sharpness. In particular, we reveal that the stronger regularization induced by Sharpness-Aware Minimizer (SAM) with unusually large neighborhood (1-SAM), improves transferability specifically, since 1-SAM and SGD have a similar natural generalization. We conclude that this strong regularization alters the exploration of the loss landscape by avoiding deep, sharp holes where the learned representation is too specific. Finally, Section 6 evaluates 1-SAM and two variants against other surrogate training procedures, and combined with nine non-training transferability techniques.

Figure 1 illustrates the insights and grounded principles to improve transferability that our contribution brings:

- The learning rate decay allows the exploration of the loss landscape to go down the valley. After a few iterations, SGD reaches its best transferability (“early stopped SGD”, gray star). The sharpness is moderate.
- As training with SGD continues, sharpness increases and transferability decreases. The fully trained model (red star) is a suboptimal surrogate. SGD falls into deep, sharp holes where the representation is too specific.
- SAM explicitly minimizes sharpness and avoids undesirable holes. Transferability is maximum after a full training (blue star) when SAM is applied over a large neighborhood (1-SAM, thick blue arrow).

## 2 RELATED WORK

**Transferability techniques.** The transferability of adversarial examples is a prolific research topic [Benz et al., 2021, Dong et al., 2018, Gubri et al., 2022a,b, Li et al., 2018, Lin et al., 2019, Springer et al., 2021, Wu et al., 2020, Xie et al., 2019, Zhao et al., 2022]. Zhao et al. [2022] suggest comparing transferability techniques within specific categories, a recommendation adhered to in Section 6. They classify gradient-based transferability techniques into four categories: model augmentation, data augmentation, attack optimizers, and feature-based attacks. Section 6 shows that our method improves these techniques when combined. Model augmentation adds randomness to the weights or the architecture to avoid specific adversarial examples: GN [Li et al., 2018] uses dropout or skip erosion, SGM [Wu et al., 2020] favors gradients from skip connections during the backward pass, LGV [Gubri et al., 2022b] collects models along the SGD trajectory during a few additional epochs with a high learning rate. Data augmentation techniques transform the inputs during the attack: DI [Xie et al., 2019] randomly resizes the input, SI [Lin et al., 2019] rescales the input, and VT [Wang and He, 2021] smooths the gradients locally. Attack optimizers smooth updates during gradient ascent with momentum (MI, Dong et al. [2018]) or Nesterov accelerated gradient (NI, Lin et al. [2019]), or minimize sharpness (RAP, [Qin et al., 2022]). RAP minimizes sharpness through a min-max bi-level optimization problem, similar to SAM but in the input space. Section 6 shows that SAM and RAP are best combined, indicating their complementary effects on two distinct factors.

**Training surrogate models.** Despite the important amount of work on transferability, the way to train an effective single surrogate base model has received little attention in the literature [Zhao et al., 2022]. Benz et al. [2021], Nitin [2021], Zhang et al. [2021] point that early stopping SGD improves transferability. Springer et al. [2021] propose SAT, slight adversarial training that uses tiny perturbations to filter out some non-robust features. Section 5 evaluates SAT. Our approach sheds new light on the relation between flatness and transferability. Springer et al. [2021] implicitly flatten the surrogate model, since adversarial trained models are flatter than their naturally trained counterparts [Stutz et al., 2021]. We observe a similar implicit link with early stopping in Section 4. Gubri et al. [2022b] propose the surrogate-target misalignment hypothesis to explain why flat minima in the weight space are better surrogate models. Section 6 shows that LGV, their model augmentation technique, is best with ours, indicating complementary effects on two distinct factors, respectively ensembling diverse representations and training a single generic representation.

**Early stopping for transferability.** Benz et al. [2021], Zhang et al. [2021], Nitin [2021] point out that fully trained

surrogate models are not optimal for transferability and propose a hypothesis based on the perspective of robust and non-robust features [Ilyas et al., 2019]. Ilyas et al. [2019] disentangles features that are highly predictive and robust to adversarial perturbations (RFs), and features that are also highly predictive but non-robust to adversarial perturbations (NRFs). A feature  $f_r$  is  $\gamma$ -robust if it remains predictive under a specified set of adversarial perturbations  $\Delta$ ,  $\mathbb{E}_{(x,y)\sim D} [\inf_{\delta\in\Delta(x)} y \cdot f_r(x + \delta)] \geq \gamma$ . A NRF  $f_{nr}$  is  $\beta$ -predictive, i.e.,  $\mathbb{E}_{(x,y)\sim D} [y \cdot f_{nr}(x)] \geq \beta$  but is not  $\gamma$ -robust feature for any  $\gamma \geq 0$ . According to Benz et al. [2021], Nitin [2021], the training of DNNs mainly learns RFs first and then learns NRFs. We term this the *RFs/NRFs evolution hypothesis* (Table 1). NRFs are transferable [Ilyas et al., 2019], but also brittle. RFs are more stable and can improve transferability [Springer et al., 2021, Zhang et al., 2021]. RFs can be attacked: RFs against  $L_p$  norm  $\varepsilon$  perturbations are vulnerable against perturbations with higher  $\varepsilon'$  or another  $L_{p'}$  norm [Springer et al., 2021, Zhang et al., 2021]. Section 3 provides some observations that tend to refute the RFs/NRFs evolution hypothesis (summary in Table 2).

**Sharpness and natural generalization.** Several training techniques increase natural generalization and reduce loss sharpness in the weight space. Keskar et al. [2017] links batch size to sharpness, defined in the weight space as  $\max_{\|e\|_2 \leq \rho} \mathcal{L}(w + e) - \mathcal{L}(w)$ . SWA [Izmailov et al., 2018] averages the weights at the last epochs for flatness. SAM [Foret et al., 2020] minimizes the maximum loss around a neighborhood by performing a gradient ascent step, defined by  $\epsilon_t = \rho \frac{\nabla \mathcal{L}(w_t)}{\|\nabla \mathcal{L}(w_t)\|_2}$ , followed by a gradient descent step,  $w_{t+1} = w_t - \alpha_t (\nabla \mathcal{L}(w_t + \epsilon_t) + \lambda w_t)$ . At the cost of one additional forward-backward pass per iteration, SAM avoids deep, sharp holes on the surface of the loss landscape [Kadour et al., 2022]. Its  $\rho$  hyperparameter controls the size of flat neighborhoods. Several variants exist that improve natural generalization [Kwon et al., 2021, Zhuang et al., 2022] or efficiency [Liu et al., 2022, Du et al., 2021] (description in Appendix E). Nevertheless, the relationship between sharpness and natural generalization is subject to scientific controversy [Andriushchenko et al., 2023, Wen et al., 2023, Bisla et al., 2022]. In Sections 5 and 6, we explore the use of SWA, SAM and six variants to train better surrogate models.

### 3 ANOTHER LOOK AT THE NON-ROBUST FEATURES HYPOTHESIS

In this section, we point the flaws of the robust and non-robust features (RFs/NRFs) evolution hypothesis Benz et al. [2021], Zhang et al. [2021], Nitin [2021] to explain the success of early stopping for transferability. They observe that early stopping the surrogate model improves the transferability. To explain this, they draw the hypothesis that DNNs

Table 1: RFs/NRFs evolution hypothesis (expected) and hypothesis based on our results (ours), about the evolution of DNN features from early stopping to full training.

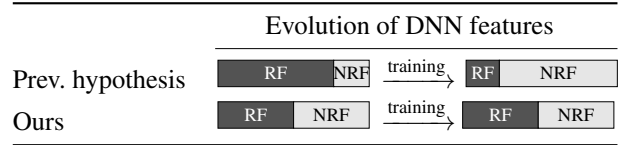


Table 2: Comparison of expected and observed evolutions of transferability from early stopped to fully trained *surrogate* model. DNN denotes a regularly trained model.

	Transferability surrogate $\mapsto$ target	Evolution of transferability	
		Expected	Observed
Fig. 2	RFs $\mapsto$ DNN		
	NRFs $\mapsto$ DNN		
Fig. 3	DNN $\mapsto$ RFs		
	DNN $\mapsto$ NRFs		

first mainly learn RFs and then NRFs (Table 1). Since RFs are less brittle than NRFs, early learned features would be more transferable than their fully trained counterparts<sup>1</sup>. We challenge the fact that DNNs first mainly learn RFs and then NRFs. Considering transferability as a proxy for representation similarity, we show no trade-off between RFs and NRFs along training epochs (see summary in Table 2). First, the transferability from RFs to a regular DNN evolve similarly as the transferability from NRFs to a regular DNN. Second, the transferabilities from a regular surrogate DNN to both RFs and NRFs target DNNs evolve similarly.

**Early stopping indeed increases transferability.** First, we check that a fully trained surrogate model is not optimal for transferability. We train two ResNet-50 surrogate models on CIFAR-10 and ImageNet using standard settings. Appendix B reports the success rates of the BIM attack applied at every epoch and evaluated on 10 fully trained target models per dataset. For both datasets and diverse targeted architectures, the optimal epoch for transferability occurs around one or two thirds of training<sup>2</sup>.

**Early stopping improves transferability from both surrogates trained on robust and non-robust features.** We show that early stopping works *similarly* well on surrogate models trained on robust and non-robust datasets. We retrieve the robust and non-robust datasets from Ilyas et al.

<sup>1</sup>Adversarial perturbations against RFs exist: either perturbations with larger  $L_p$  norms  $\varepsilon$ , or with another  $L_{p'}$  norm, as chosen by Springer et al. [2021], Zhang et al. [2021].

<sup>2</sup>Transferability decreases along epochs, except for the two vision transformers targets on ImageNet where the transferability is stable at the end of training.

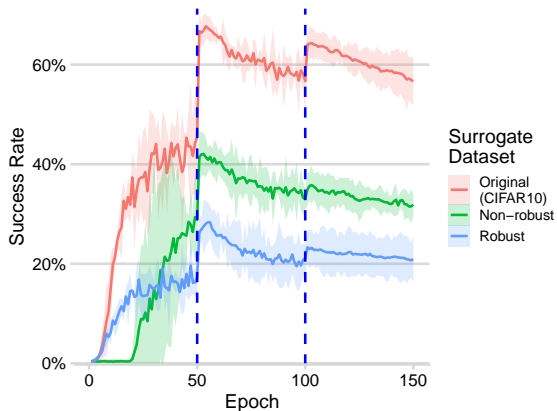


Figure 2: Early stopping improves the transferability *from* surrogate models trained on both robust and non-robust datasets. Average success rate evaluated over ten target models trained on the original CIFAR-10 dataset, from a ResNet-50 surrogate model trained for a number of epochs (x-axis) on the datasets  $D_R$  (blue) and  $D_{NR}$  (green) of Ilyas et al. [2019] modified from CIFAR-10 (red). We craft all adversarial examples from the same subset of the original CIFAR-10 test set. Average (line) and confidence interval of  $\pm$  two standard deviations (colored area) of three training runs. Appendix C contains the details per target.

[2019], that are altered from CIFAR-10 to mostly contain RFs and, respectively, NRFs. We train two ResNet-50 models on both datasets with SGD (hyperparameters reported in Appendices B and C). Figure 2 shows the transferability across training epochs, averaged over the ten regularly trained targets. The success rates of both robust and non-robust surrogate models evolve similarly to the model trained on the original dataset: transferability peaks around the epochs 50 and 100 and decreases during the following epochs. This observation is valid for all ten targets (Appendix C). According to the RFs/NRFs evolution hypothesis, we expect “X-shaped” transferability curves: if DNNs first mainly learn RFs and then NRFs, the transferability from NRFs would increase and the transferability from RFs would strictly decrease (from early stopping to full training). The RFs/NRFs hypothesis does not describe why early learned NRFs are better to target a regular DNN than fully learned NRFs.

**Early stopping improves transferability to both targets trained on robust and non-robust features.** We observe that an early stopped surrogate model trained on the original dataset is best to target both RFs and NRFs targets. Here, we keep the original CIFAR-10 dataset to train the surrogate model. We target four ResNet-50 models trained on the robust and non-robust datasets of Ilyas et al. [2019]<sup>3</sup>. Figure 3

<sup>3</sup>In this experiment, we include two additional non-robust datasets  $D_{rand}$  and  $D_{det}$  from Ilyas et al. [2019]. By construction,

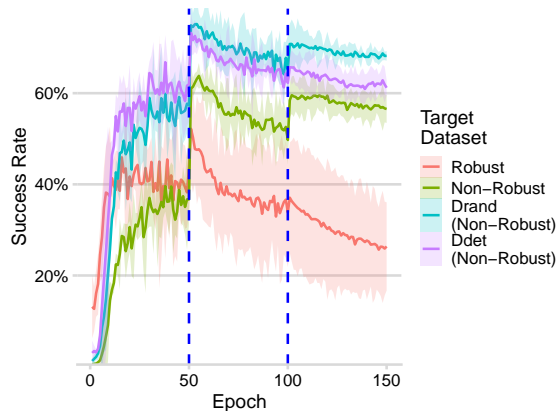


Figure 3: Early stopping improves the transferability *to* target models trained on both robust and non-robust datasets. Success rate from a ResNet-50 trained for a number of epochs (x-axis) on the original CIFAR-10 dataset, to ResNet-50 targets trained on the robust dataset  $D_R$  (red), and the three non-robust datasets  $D_{NR}$  (green),  $D_{rand}$  (blue) and  $D_{det}$  (purple) of Ilyas et al. [2019] modified from CIFAR-10. The perturbation norm  $\epsilon$  is  $\frac{16}{255}$  for the  $D_R$  target,  $\frac{2}{255}$  for the  $D_{NR}$  target and  $\frac{1}{255}$  for the  $D_{rand}$  and  $D_{det}$  targets to adapt to the vulnerability of target models (the order of lines cannot be compared). Average (line) and confidence interval of  $\pm$  two standard deviations (colored area) of three training runs.

shows that the same epoch of standard training is optimal for attacking all four models, i.e., composed of either RFs or NRFs. The RFs/NRFs evolution hypothesis fails to explain why early stopping is best to target NRFs.

Overall, we provide new evidence that early stopping for transferability acts similarly on robust and non-robust features. We do not observe an inherent trade-off between RFs and NRFs. Since the higher the transferability, the more similar the representations are, we conclude that the early trained representations are more similar to both RFs and NRFs than their fully trained counterparts. Therefore, the hypothesis that early stopping favors RFs over NRFs does not hold. We conjecture that a phenomenon orthogonal to RFs/NRFs explains why fully trained surrogates are not optimal.

## 4 STOPPING EARLIER: TRANSFERABILITY AND TRAINING DYNAMICS

This section investigates the link between surrogate model training dynamics and transferability, highlighting that transferability peaks when sharpness drops.

their *only* useful features for classification are NRFs. They were excluded from the previous experiment due to training instability.

**Transferability peaks when the LR decays.** The optimal number of surrogate training epochs for transferability occurs just after the decay of the LR. We train a ResNet-50 surrogate model for 150 epochs on CIFAR-10, using the standard LR schedule of Engstrom et al. [2019] which divides the LR by 10 at epochs 50 and 100. For the ten targets considered individually, the highest transferability is between epochs 51 and 55 (Appendix B). Figure 4 shows that transferability suddenly peaks after both LR decays (red line). We observe the same phenomenon on ImageNet<sup>4</sup>. Overall, the success of early stopping appears to be related to the exploration of the loss landscape, which is governed by the learning rate.

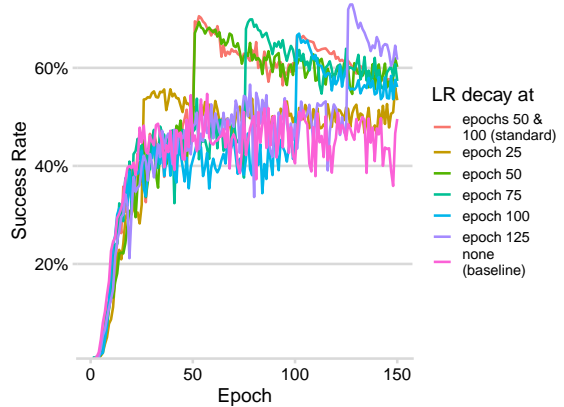


Figure 4: Transferability peaks when the learning rate decays at any epochs. Average success rate evaluated over ten target models from a ResNet-50 surrogate model trained for a number of epochs (x-axis) on CIFAR-10. The learning rate is divided by 10 once during training at the epoch corresponding to the color. Red is our standard schedule, with two decays at epochs 50 and 100. Pink is the baseline of constant learning rate. Best seen in colors.

**Consistency of the peak of transferability across training.** This peak of transferability can be consistently observed at any point of training. Here, we modify the standard double decay LR schedule to perform a single decay at a specified epoch. The learning rate is constant (0.1) until the specified epoch, where it is ten times lower for the rest of the training. We evaluate the transferability of five surrogates with a decay at, respectively, epoch 25, 50, 75, 100 and 125. Figure 4 reports a similar transferability peak for all these surrogates, except for the smaller peak at epoch 25 where the decay occurs before the end of the initial convergence. The consistency of the peak of transferability across training epochs is valid for all individual targets (Appendix D). As a baseline, we use a constant learning rate, under which transferability plateaus without any observed peak. Therefore, we conclude that the step decay of the LR enables early stopping to improve transferability.

**Sharpness drops when the LR decays.** When the LR decays, the sharpness in the weight space drops. Figure 5 reports two sharpness metrics per the training epoch of our standard CIFAR-10 surrogate: the largest Hessian eigenvalue measures the sharpness of the sharpest direction in the weight space (red, worst-case sharpness) and the Hessian trace measures the total sharpness of all weight space directions (blue, average sharpness). Both types of sharpness decrease abruptly, significantly and immediately after both LR decays. Simultaneously, transferability peaks (orange).

We conclude that the effect of early stopping on transferability is tightly related to the dynamics of the exploration of the loss surface, governed by the learning rate. Overall, Figure 1 illustrates our observations:

1. Before the LR decays, the training bounces back and forth crossing the valley from above (top gray arrows).

<sup>4</sup>On ImageNet, we train a ResNet-50 surrogate for 90 epochs with LR decays at epochs 30 and 60. The highest transferability per target occurs either after the first decay (epochs 31 or 35) or after the second one (epochs 62 or 67), except for both vision transformer targets, where transferability plateaus at a low success rate after the second decay.

For an extended discussion, see Appendix D.

2. After the LR decays, training goes down the valley. Soon after, SGD has its best transferability (“early stopped SGD” gray star). Sharpness is reduced.
3. As training continues, the loss decreases while sharpness slowly increases. SGD settles into a “deep hole” in the loss landscape, with specific representations of low transferability (“fully trained SGD” red star).

## 5 GOING FURTHER: FLATNESS AT THE RESCUE OF SGD

Since transferability peaks to its higher value when sharpness drops, we now explore how to improve transferability by minimizing the sharpness of the surrogate model. First, we show that seven training techniques that minimize both the loss value and the loss sharpness can train better surrogate models. Second, we uncover that SAM (and five variants) with unusually large flat neighborhoods induces a stronger regularization that specifically increases transferability.

**Minimizing sharpness improves transferability.** The training techniques known to decrease the sharpness of the models train better surrogate representations. We evaluate the transferability of seven training techniques belonging to two families, SWA and SAM (see Section 2 and Appendix A for a more detailed presentation). SWA [Izmailov et al., 2018] decreases sharpness implicitly by averaging the weights collected by SGD. Our SWA surrogate is the average of the weights obtained by our standard SGD surrogate

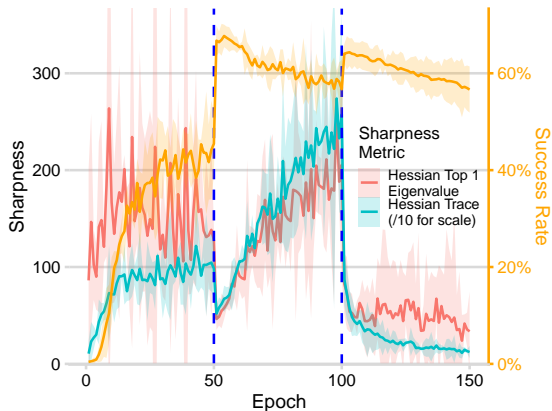


Figure 5: Sharpness drops when the learning rate decays. Largest eigenvalue of the Hessian (red) and trace of the Hessian (blue) for all training epochs (x-axis) on CIFAR-10. Average success rate on ten targets (orange, right axis). Average (line) and confidence interval of  $\pm$  two standard deviations (colored area) of three training runs. Vertical bars indicate the learning rate step decays. Best seen in colors.

at the end of the last 25% epochs<sup>5</sup>. Figure 6 shows that SWA (yellow) improves the success rate compared to fully trained SGD (red) on both datasets. On ImageNet, SWA beats the early stopped SGD surrogate, but not on CIFAR-10. Indeed, SWA helps to find flatter solutions than those found by SGD, but SWA is confined to the same basin of attraction [Kaddour et al., 2022]. To remediate to this issue, we also train several surrogate models with SAM [Foret et al., 2020] and its variants, i.e., GSAM [Zhuang et al., 2022], ASAM [Kwon et al., 2021], AGSAM (GSAM+ASAM), WASAM (SAM+SWA, Kaddour et al. [2022]), and LookSAM [Liu et al., 2022]. SAM explicitly minimizes sharpness during training by solving a min-max optimization problem. At each iteration step, SAM first maximizes the loss in a neighborhood to compute a second gradient that is used to minimize the loss (details in Appendix E). We train one model per SAM variant using the original SAM hyperparameter ( $\rho = 0.05$ ). Figure 6 shows that SAM and its variants (dotted lines) train surrogate models that have a significantly higher transferability than fully trained SGD, early stopped SGD and SWA, on both datasets. On ImageNet, the success rate of SAM averages over the ten targets at 18.7%, compared to 13.3% for full training with SGD, 14.5% for SGD at its best (epoch 66) and 15.2% for SWA, and respectively 77.3%, 56.6%, 67.7% (epoch 54) and 60.5% on CIFAR-10. SAM finds different basins of attractions than SGD [Foret et al., 2020, Kaddour et al., 2022]. Therefore, some basins of attraction are better surrogate than others, and explicitly minimizing sharpness reaches better ones.

<sup>5</sup>We also update the batch-normalization statistics of the SWA model with one forward pass over the training data on CIFAR-10 (10% on ImageNet).

### Strong regularization from large flat neighborhoods significantly improves transferability.

We uncover that the size of the flat neighborhood of SAM and its variants induces a regularization that is tightly linked to transferability. We observe that SAM and its variants with uncommonly large flat neighborhoods train significantly and consistently better surrogate models. SAM seeks neighborhoods with uniformly low loss of size controlled by its  $\rho$  hyperparameter (Section 2). We tune it on CIFAR-10 on distinct validation sets of natural examples, target, and surrogate models (details in Appendix E). For all SAM variants, the optimal  $\rho$  for transferability is always larger than the original  $\rho$ , and unusually large compared to the range of values used for natural accuracy. Indeed, we find  $\rho$  of 0.3 optimal for SAM, and Foret et al. [2020] originally uses  $\rho$  of 0.05. Kaddour et al. [2022] and Zhuang et al. [2022] tune  $\rho$  with a maximum of, respectively, 0.2 and 0.3. Figure 6 reports the transferability of SAM and its variants with both the original  $\rho$  (dotted) and with the larger  $\rho$  found optimal on CIFAR-10 (plain). All SAM variants train a better surrogate model with large  $\rho$  values<sup>6</sup>. In the following, we denote **I-SAM** for SAM with large  $\rho$  (0.3), and similarly **I-AGSAM** and **I-LookSAM** (respectively, 4<sup>7</sup> and 0.3). Kaddour et al. [2022] show that changing  $\rho$  ends up in different basins of attraction. Therefore, the stronger regularization induced by I-SAM avoids large sharp holes on top of the loss surface, and significantly improves transferability.

### The benefits of the strong regularization from large flat neighborhoods are specific to transferability.

The stronger regularization of SAM with a large value of  $\rho$  is specifically related to transferability. First, this strength of regularization may degrade natural accuracy. On ImageNet with ResNet-18, the top-1 accuracy of SAM with large  $\rho$  is equal to 67.89%, less than SAM with the original  $\rho$  (70.29%) and even less than fully trained SGD (69.84%). This observation extends to ResNet-50 and to the other variants of SAM on ImageNet (Appendix E). Therefore, the improvement in generalization of adversarial examples cannot be explained by an improvement in natural generalization (better fit to the data). Second, unlike SAM, a stronger regularization of weight decay decreases transferability, showing a specific relation between transferability and SAM. We train multiple surrogate models using SGD with different values of weight decay. The optimal weight decay value for the ResNet-50 surrogate is the same value used to train the target model (see Appendix F for details). Therefore, not all regularization schemes help to train a better surrogate model.

<sup>6</sup>As expected, LookSAM shows a slower learning behavior over the epoch, compared to other SAM variants: LookSAM is an efficient variant that computes the additional SAM gradient only once each five optimizer iteration.

<sup>7</sup>I-AGSAM uses  $\rho$  value of 4, since as suggested by Kwon et al. [2021] adaptive variants should use  $\rho$  10 times larger. We found our observations consistent with this recommendation.

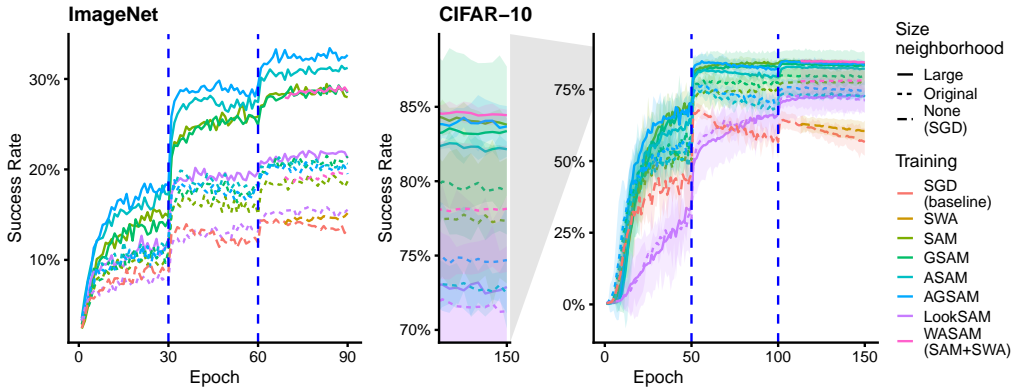


Figure 6: SAM variants and SWA improve transferability over SGD, and SAM with large neighborhoods over the original SAM. Average success rate evaluated over ten target models from a ResNet-18 surrogate model trained for a number of epochs (x-axis) on ImageNet (left), and from a ResNet-50 on CIFAR-10 (right). SAM and its variants are trained with both the original size of flat neighborhood (dotted,  $\rho = 0.05$  except  $\rho = 0.5$  for adaptive variants) and the larger size that we tuned for transferability (plain). Red is our standard SGD surrogate. Best seen in colors.

Overall, the sharpness of the surrogate model is tightly related to transferability:

- Minimizing implicitly or explicitly the loss sharpness trains better surrogate models.
- The strong SAM regularization avoids deep sharp minima in favor of unusually large flat neighborhoods that contain more generic representations.
- The stronger SAM regularization is tailored for transferability: it can reduce natural accuracy, and other strong regularization schemes, such as weight decay, do not aid in transferability.

## 6 PUTTING IT ALL TOGETHER: IMPROVING TRANSFERABILITY TECHNIQUES WITH SHARPNESS MINIMIZATION

In this section, we show that explicitly minimizing sharpness is a competitive technique for training surrogate models and complements well other transferability techniques. To benchmark our principle against related work, we adhere to the best practices suggested by Zhao et al. [2022]. Specifically, we evaluate the benefits of minimizing sharpness on large neighborhoods against other surrogate training techniques (same category), and also assess their complementarity with techniques from distinct categories. All our code and models are available on GitHub<sup>8</sup>.

**Minimizing sharpness improves over competitive techniques.** l-SAM and l-AGSAM are competitive alternatives

<sup>8</sup><https://github.com/Framartin/rfn-flatness-transferability>

to existing surrogate training techniques, and l-LookSAM offers good transferability for a small computational overhead. For a fair comparison, we choose the epoch of the early stopped SGD surrogate by evaluating a validation transferability at every training epoch<sup>9</sup>. We retrieve the SAT (Slight Adversarial Training) ImageNet weights used by Springer et al. [2021], and we train SAT on CIFAR-10 using their hyperparameters. Table 3 reports the average success rate of the aforementioned techniques, alongside their computational overhead. This overhead is the ratio of forward-backward passes needed by the training technique to those required by SGD. On both datasets, l-AGSAM is the best surrogate. l-AGSAM beats the transferability of SAT, while dividing the training cost by two on ImageNet and four on CIFAR-10. Nevertheless, l-AGSAM doubles the computational number of forward-backward passes compared to SGD. By computing the additional SAM gradient only once per five iterations, l-LookSAM is a viable alternative to contain the computational overhead to 1.23, while having higher transferability than SGD. Overall, sharpness-aware minimizers with large flat neighborhoods offer a good trade-off between transferability and computation.

**Minimizing sharpness trains better base models for complementary techniques.** l-SAM is a good base model to combine with existing model augmentation, data augmentation, and attack optimization transferability techniques. These categories aim complementary objectives: model and data augmentations reduce the tendency of the attack to overfit the base model by adding randomness to gradients. Attack optimizers intend to smooth the gradient updates.

<sup>9</sup>To avoid data leakage that violates our no-query threat model, we craft one thousand adversarial examples from images of a validation set and evaluate them on a distinct set of target models.

Table 3: Success rate and computation cost of surrogate training techniques on ImageNet and CIFAR-10. Average success rate on ten targets from a ResNet-50 surrogate with a maximum perturbation  $L_\infty$  norm  $\varepsilon$  of  $4/255$  (other norms in Appendix). The computational overhead is relative to the number of SGD forward-backward passes. Bold is best. In %.

Surrogate	Success Rate $\uparrow$		Computation Cost $\downarrow$	
	ImageNet	CIFAR-10	ImageNet	CIFAR-10
Fully Trained SGD	17.81	56.06	$\times 1$	$\times 1$
Early Stopped SGD	19.97	70.16	$\times 0.77$	$\times 0.36$
SAT [Springer et al., 2021]	49.74	62.45	$\times 4$	$\times 8$
SWA	20.83	60.26	$\times 1.00$	$\times 1.00$
l-SAM (ours)	48.75	85.50	$\times 2$	$\times 2$
l-AGSAM (ours)	<b>53.14</b>	<b>85.72</b>	$\times 2$	$\times 2$
l-LookSAM (ours)	34.92	77.49	$\times 1.23$	$\times 1.22$

Table 4: Success rate of other categories of transferability techniques applied on the standard SGD base surrogate and on our l-SAM base surrogate. Average success rate on our ten ImageNet targets from ResNet-50 models with a maximum perturbation  $L_\infty$  norm  $\varepsilon$ . Bold is best. In %.

Attack	$\varepsilon = 2/255$		$\varepsilon = 4/255$		$\varepsilon = 8/255$	
	SGD	l-SAM	SGD	l-SAM	SGD	l-SAM
<b>Model Augmentation Techniques</b>						
GN [Li et al., 2018]	12.9	<b>28.8</b>	27.8	<b>52.8</b>	46.5	<b>71.0</b>
SGM [Wu et al., 2020]	11.7	<b>24.3</b>	29.3	<b>51.5</b>	55.6	<b>76.2</b>
LGV [Gubri et al., 2022b]	24.8	<b>25.2</b>	53.5	<b>54.7</b>	72.1	<b>73.7</b>
<b>Data Augmentation Techniques</b>						
DI [Xie et al., 2019]	22.1	<b>42.0</b>	47.0	<b>72.5</b>	69.4	<b>86.9</b>
SI [Lin et al., 2019]	10.8	<b>28.8</b>	26.9	<b>56.7</b>	49.9	<b>77.2</b>
VT [Wang and He, 2021]	10.5	<b>31.9</b>	24.9	<b>59.4</b>	43.0	<b>78.5</b>
<b>Attack Optimizers</b>						
MI [Dong et al., 2018]	12.3	<b>32.0</b>	26.8	<b>59.6</b>	46.3	<b>78.3</b>
NI [Lin et al., 2019]	8.3	<b>20.6</b>	22.3	<b>46.5</b>	43.9	<b>70.5</b>
RAP [Qin et al., 2022]	11.5	<b>30.1</b>	26.2	<b>56.2</b>	42.8	<b>74.7</b>

Table 4 reports the success rate of nine transferability techniques combined with our l-SAM base model on ImageNet. For all perturbation norms  $\varepsilon$ , l-SAM provides a base model that improves every nine techniques, compared to the standard fully trained SGD surrogate, from 0.4 to 35.5 percentage points. RAP [Qin et al., 2022]) is particularly interesting, since RAP minimizes sharpness like SAM but in the input space. SAM and RAP are best combined, indicating their complementary effects on two distinct factors: SAM finds generic representations, while RAP finds adversarial examples that do not overfit a single representation.

## 7 CONCLUSION

Overall, our insights into the behavior of SGD through the lens of transferability drive us to a successful approach to train better surrogate models with limited computational

overhead. We reject the hypothesis that early stopping benefits transferability due to an inherent trade-off between robust and non-robust features. Instead, we explain the success of early stopping in relation to the dynamics of the exploration of the loss landscape, focusing on sharpness. SGD drives down the valley and progressively falls into deep, sharp holes. These fully trained representations are too specific to generate highly transferable adversarial examples. We remediate this issue by minimizing sharpness. The strong SAM regularization from large flat neighborhoods closely links with transferability. Avoiding large sharp holes proves useful in improving transferability on its own and in complement with existing transferability techniques. Future research could investigate the relationship between transferability and the secondary effects of minimizing sharpness [Bisla et al., 2022, Andriushchenko et al., 2023, Wen et al., 2023].

## Acknowledgements

This work is supported by the Luxembourg National Research Funds (FNR) through CORE project C18/IS/12669767/STELLAR/LeTraon. This work was also supported by NAVER Corporation.

## References

- Maksym Andriushchenko, Francesco Croce, Maximilian Müller, Matthias Hein, and Nicolas Flammarion. A modern look at the relationship between sharpness and generalization. February 2023.
- Arsenii Ashukha, Alexander Lyzhov, Dmitry Molchanov, and Dmitry Vetrov. Pitfalls of In-Domain Uncertainty Estimation and Ensembling in Deep Learning. 2 2020. URL <http://arxiv.org/abs/2002.06470>.
- Philipp Benz, Chaoning Zhang, and In So Kweon. Batch Normalization Increases Adversarial Vulnerability and Decreases Adversarial Transferability: A Non-Robust Feature Perspective. In *ICCV 2021*, 10 2021. doi: 10.1109/ICCV48922.2021.00772. URL <http://arxiv.org/abs/2010.03316>.
- Battista Biggio, Igino Corona, Davide Maiorca, Blaine Nelson, Nedim Šrđić, Pavel Laskov, Giorgio Giacinto, and Fabio Roli. Evasion attacks against machine learning at test time. In *Lecture Notes in Computer Science (including subseries Lecture Notes in Artificial Intelligence and Lecture Notes in Bioinformatics)*, volume 8190 LNAI, pages 387–402, 8 2013. ISBN 9783642409936. doi: 10.1007/978-3-642-40994-3\_{\\_}25. URL <http://arxiv.org/abs/1708.06131>[http://dx.doi.org/10.1007/978-3-642-40994-3\\_25](http://dx.doi.org/10.1007/978-3-642-40994-3_25).
- Devansh Bisla, Jing Wang, and Anna Choromanska. Low-pass filtering sgd for recovering flat optima in the deep learning optimization landscape. In Gustau Camps-Valls, Francisco J. R. Ruiz, and Isabel Valera, editors, *Proceedings of The 25th International Conference on Artificial Intelligence and Statistics*, volume 151 of *Proceedings of Machine Learning Research*, pages 8299–8339. PMLR, 28–30 Mar 2022. URL <https://proceedings.mlr.press/v151/bisla22a.html>.
- Yinpeng Dong, Fangzhou Liao, Tianyu Pang, Hang Su, Jun Zhu, Xiaolin Hu, and Jianguo Li. Boosting Adversarial Attacks with Momentum. In *Proceedings of the IEEE Computer Society Conference on Computer Vision and Pattern Recognition*, pages 9185–9193, 10 2018. ISBN 9781538664209. doi: 10.1109/CVPR.2018.00957. URL <http://arxiv.org/abs/1710.06081>.
- Jiawei Du, Hanshu Yan, Jiashi Feng, Joey Tianyi Zhou, Liangli Zhen, Rick Siow Mong Goh, and Vincent Tan. Efficient Sharpness-aware Minimization for Improved Training of Neural Networks. In *International Conference on Learning Representations*, October 2021.
- Logan Engstrom, Andrew Ilyas, Shibani Santurkar, and Dimitris Tsipras. Robustness (Python Library), 2019. URL <https://github.com/MadryLab/robustness>.
- Pierre Foret, Ariel Kleiner Google Research, Hossein Mobahi Google Research, and Behnam Neyshabur Blueshift. Sharpness-Aware Minimization for Efficiently Improving Generalization. 10 2020. doi: 10.48550/arxiv.2010.01412. URL <https://arxiv.org/abs/2010.01412v3>.
- Ian J. Goodfellow, Jonathon Shlens, and Christian Szegedy. Explaining and Harnessing Adversarial Examples. 12 2014. URL <http://arxiv.org/abs/1412.6572>.
- Martin Gubri, Maxime Cordy, Mike Papadakis, Yves Le Traon, and Koushik Sen. Efficient and Transferable Adversarial Examples from Bayesian Neural Networks. In *UAI 2022*, 2022a. URL <http://arxiv.org/abs/2011.05074>.
- Martin Gubri, Maxime Cordy, Mike Papadakis, Yves Le Traon, and Koushik Sen. LGV: Boosting Adversarial Example Transferability from Large Geometric Vicinity. In *ECCV 2022*, 2022b.
- Andrew Ilyas, Shibani Santurkar, Dimitris Tsipras, Logan Engstrom, Brandon Tran, and Aleksander Madry. Adversarial Examples Are Not Bugs, They Are Features. 5 2019. URL <http://arxiv.org/abs/1905.02175>.
- Pavel Izmailov, Dmitrii Podoprikin, Timur Garipov, Dmitry Vetrov, and Andrew Gordon Wilson. Averaging weights leads to wider optima and better generalization. In *34th Conference on Uncertainty in Artificial Intelligence 2018, UAI 2018*, volume 2, pages 876–885. Association For Uncertainty in Artificial Intelligence (AUAI), March 2018. ISBN 978-1-5108-7160-1.
- Jean Kaddour, Linqing Liu, Ricardo Silva, and Matt J. Kusner. When Do Flat Minima Optimizers Work? In *NeurIPS 2022*, 2 2022. doi: 10.48550/arxiv.2202.00661. URL <https://arxiv.org/abs/2202.00661v5>.
- Nitish Shirish Keskar, Dheevatsa Mudigere, Jorge Nocedal, Mikhail Smelyanskiy, and Ping Tak Peter Tang. On large-batch training for deep learning: Generalization gap and sharp minima. In *International Conference on Learning Representations*, 2017. URL <https://openreview.net/forum?id=H1oyR1Ygg>.
- Hoki Kim. Torchattacks: A pytorch repository for adversarial attacks. *arXiv preprint arXiv:2010.01950*, 2020.

- Alexey Kurakin, Ian J. Goodfellow, and Samy Bengio. Adversarial examples in the physical world. In *5th International Conference on Learning Representations, ICLR 2017 - Workshop Track Proceedings*, 7 2017. URL <http://arxiv.org/abs/1607.02533>.
- Jungmin Kwon, Jeongseop Kim, Hyunseo Park, and In Kwon Choi. ASAM: Adaptive Sharpness-Aware Minimization for Scale-Invariant Learning of Deep Neural Networks. 2 2021. doi: 10.48550/arxiv.2102.11600. URL <https://arxiv.org/abs/2102.11600v3>.
- Yingwei Li, Song Bai, Yuyin Zhou, Cihang Xie, Zhishuai Zhang, and Alan Yuille. Learning Transferable Adversarial Examples via Ghost Networks. *Proceedings of the AAAI Conference on Artificial Intelligence*, 34(07): 11458–11465, 12 2018. ISSN 2374-3468. doi: 10.1609/aaai.v34i07.6810. URL <http://arxiv.org/abs/1812.03413>.
- Jiadong Lin, Chuanbiao Song, Kun He, Liwei Wang, and John E. Hopcroft. Nesterov Accelerated Gradient and Scale Invariance for Adversarial Attacks. 8 2019. URL <http://arxiv.org/abs/1908.06281>.
- Yong Liu, Siqi Mai, Xiangning Chen, Cho-Jui Hsieh, and Yang You. Towards Efficient and Scalable Sharpness-Aware Minimization. In *CVPR*, pages 12360–12370, 2022.
- Muzammal Naseer, Kanchana Ranasinghe, Salman Khan, Fahad Shahbaz Khan, and Fatih Porikli. On Improving Adversarial Transferability of Vision Transformers. In *ICLR (spotlight)*, 3 2022.
- Vikram Nitin. SGD on Neural Networks learns Robust Features before Non-Robust, 3 2021.
- Zeyu Qin, Yanbo Fan, Yi Liu, Li Shen, Yong Zhang, Jue Wang, and Baoyuan Wu. Boosting the Transferability of Adversarial Attacks with Reverse Adversarial Perturbation. In *NeurIPS 2022*, October 2022. doi: 10.48550/arxiv.2210.05968.
- Frank Schneider, Felix Dangel, and Philipp Henning. Cockpit: A Practical Debugging Tool for the Training of Deep Neural Networks. 2 2021. doi: 10.48550/arxiv.2102.06604. URL <https://arxiv.org/abs/2102.06604v2><https://arxiv.org/abs/2102.06604>.
- Jacob M. Springer, Melanie Mitchell, and Garrett T. Kenyon. A Little Robustness Goes a Long Way: Leveraging Robust Features for Targeted Transfer Attacks. *Advances in Neural Information Processing Systems*, 12:9759–9773, 6 2021. ISSN 10495258. doi: 10.48550/arxiv.2106.02105. URL <https://arxiv.org/abs/2106.02105v2>.
- David Stutz, Matthias Hein, and Bernt Schiele. Relating Adversarially Robust Generalization to Flat Minima. *Proceedings of the IEEE International Conference on Computer Vision*, pages 7787–7797, 4 2021. ISSN 15505499. doi: 10.1109/ICCV48922.2021.00771. URL <https://arxiv.org/abs/2104.04448v2>.
- Christian Szegedy, Wojciech Zaremba, Ilya Sutskever, Joan Bruna, Dumitru Erhan, Ian Goodfellow, and Rob Fergus. Intriguing properties of neural networks. 12 2013. URL <http://arxiv.org/abs/1312.6199>.
- Xiaosen Wang and Kun He. Enhancing the Transferability of Adversarial Attacks through Variance Tuning. *Proceedings of the IEEE Computer Society Conference on Computer Vision and Pattern Recognition*, pages 1924–1933, 3 2021. ISSN 10636919. doi: 10.1109/CVPR46437.2021.00196. URL <https://arxiv.org/abs/2103.15571v3>.
- Kaiyue Wen, Zhiyuan Li, and Tengyu Ma. Sharpness Minimization Algorithms Do Not Only Minimize Sharpness To Achieve Better Generalization, July 2023.
- Dongxian Wu, Yisen Wang, Shu-Tao Xia, James Bailey, and Xingjun Ma. Skip Connections Matter: On the Transferability of Adversarial Examples Generated with ResNets. In *ICLR*, 2 2020. URL <https://arxiv.org/abs/2002.05990v1><https://arxiv.org/abs/2002.05990>.
- Cihang Xie, Zhishuai Zhang, Yuyin Zhou, Song Bai, Jiayu Wang, Zhou Ren, and Alan L. Yuille. Improving transferability of adversarial examples with input diversity. In *Proceedings of the IEEE Computer Society Conference on Computer Vision and Pattern Recognition*, volume 2019-June, pages 2725–2734, 3 2019. ISBN 9781728132938. doi: 10.1109/CVPR.2019.00284. URL <http://arxiv.org/abs/1803.06978>.
- Zhewei Yao, Amir Gholami, Kurt Keutzer, and Michael W. Mahoney. PyHessian: Neural Networks Through the Lens of the Hessian. *Proceedings - 2020 IEEE International Conference on Big Data, Big Data 2020*, pages 581–590, 12 2019. ISSN 2331-8422. doi: 10.1109/BigData50022.2020.9378171. URL <https://arxiv.org/abs/1912.07145v3>.
- Chaoning Zhang, Gyusang Cho, Philipp Benz, Kang Zhang, Chenshuang Zhang, Chan-Hyun Youn, and In So Kweon. Early Stop And Adversarial Training Yield Better surrogate Model: Very Non-Robust Features Harm Adversarial Transferability, 2021.
- Zhengyu Zhao, Hanwei Zhang, Renjue Li, Ronan Sicre, Laurent Amsaleg, and Michael Backes. Towards Good Practices in Evaluating Transfer Adversarial Attacks. 11 2022. doi: 10.48550/arxiv.2211.09565. URL <https://arxiv.org/abs/2211.09565v1>.

Juntang Zhuang, Boqing Gong, Liangzhe Yuan, Yin Cui, Hartwig Adam, Nicha C Dvornek, sekhar tatikonda, James s Duncan, and Ting Liu. Surrogate Gap Minimization Improves Sharpness-Aware Training. In *International Conference on Learning Representations, 2022*. URL <https://openreview.net/forum?id=edONMAnhLu->.

---

# Going Further: Flatness at the Rescue of Early Stopping for Adversarial Example Transferability (Supplementary Material)

---

Martin Gubri<sup>§§ 1</sup>

Maxime Cordy<sup>2</sup>

Yves Le Traon<sup>2</sup>

<sup>1</sup>Parameter Lab, Tübingen, Germany

<sup>2</sup>University of Luxembourg, Luxembourg, Luxembourg

These supplementary materials contain the following sections:

- Appendix A details the experimental settings,
- Appendix B reports the transferability and the natural accuracy by epochs of surrogate trained with SGD on CIFAR-10 and ImageNet,
- Appendix C reports additional results of Section 3 “Another Look at the Non-Robust Features Hypothesis about Early Stopping”,
- Appendix D reports additional results of Section 4 “Stopping Earlier: Transferability and Training Dynamics”,
- Appendix E reports additional results of Section 5 “Going Further: Flatness At The Rescue of SGD”,
- Appendix F reports the results about transferability with respect to the weight decay of the surrogate,
- Appendix G reports additional results of Section 6 “Putting It All Together: Improving Transferability Techniques With Sharpness Minimization”.

## A EXPERIMENTAL SETTINGS

This section describes the experimental settings used in this article. The experimental setup is standard for transfer-based attacks.

- Our source code used to train and evaluate models is publicly available on GitHub at this URL: <https://github.com/Framartin/rfn-flatness-transferability>.
- Our trained models on both CIFAR-10 and ImageNet are publicly distributed through HuggingFace at this URL: <https://huggingface.co/mgubri/rfn-flatness-transferability>.

**Target models.** All our target models on CIFAR-10 are fully trained for 150 epochs with SGD using the hyperparameters reported in Table 5. For a fair comparison, *the baseline surrogate is trained with SGD using the same hyperparameters as the targets*. On CIFAR-10, we target the following ten architectures: ResNet-50 (the surrogate with the same architecture is an independently trained model), ResNet-18, ResNet-101, DenseNet-161, DenseNet-201, WideResNet-28-10, VGG13, VGG19, Inception v3 and ConvMixer. On ImageNet, the target models are the pretrained models distributed by PyTorch. The ten target architectures on ImageNet are the following: ResNet-50, ResNet-152, ResNeXt-50 32X4D, WideResNet-50-2, DenseNet-201, VGG19, GoogLeNet (Inception v1), Inception v3, ViT B 16 and Swin S. Additionally, we train a “validation” set of architectures on CIFAR-10 to select hyperparameters independently of reported results. This set is composed of: ResNet-50 (another independently trained model), ResNet-34, ResNet-152, DenseNet-121, DenseNet-169, WideResNet-16-8, VGG11, VGG16, GoogLeNet (Inception v1) and MLP Mixer. This validation set of target models on ImageNet is composed of the following architectures: ResNet-50 (another independently trained model), ResNet-101, ResNeXt-101 64X4D, WideResNet101-2, VGG16, DenseNet121, ViT B 32 and Swin B.

---

<sup>\*</sup>Work conducted during the author’s PhD at the University of Luxembourg.

<sup>§§</sup>Work conducted during the author’s PhD at the University of Luxembourg.

**Surrogate models trained with SGD.** We train the surrogate models on CIFAR-10 and ImageNet using SGD with the standard hyperparameters of the robustness library [Engstrom et al., 2019] (Table 5). Due to computational limitations on ImageNet, we limit the number of epochs to 90, reusing the same hyperparameters as Ashukha et al. [2020].

**Surrogate models trained with SAM and its variants.** We train surrogate models with SAM using the same hyperparameters as the models trained with SGD for both datasets. We integrate the SAM optimizer into the robustness library Engstrom et al. [2019]. The unique hyperparameter of SAM is  $\rho$ , which is set to 0.05 as the original paper for both datasets for the original SAM surrogate. Our SAM surrogate with large flat neighborhoods, called l-SAM, is trained with SAM with  $\rho$  equal to 0.4. The  $\rho$  values used to train the variants of SAM are reported in Table 5. We use official or popular implementations of ASAM [Kwon et al., 2021], GSAM [Zhuang et al., 2022], AGSAM (GSAM+ASAM), LookSAM [Liu et al., 2022] and WASAM (SAM+SWA, Kaddour et al. [2022]), following the original papers. LookSAM is an efficient variant of SAM that computes the additional gradient of SAM only once per five training iterations. As reported by Liu et al. [2022], LookSAM is unstable at the beginning of training. Liu et al. [2022] solve this issue using a learning rate with warmup. Since we wanted to use the same learning rate schedule for all training techniques, we added another type of warmup. LookSAM computes the additional SAM gradient at all training iterations during the first three epochs. Our LookSAM is equivalent to SAM before the fourth epoch. This simple solution is enough for LookSAM to converge. This computational overhead is taken into account in the computational cost reported in Table 3.

**Other surrogate training techniques (Section 6).** To compare with competitive training techniques on ImageNet, we retrieve the original models of SAT Springer et al. [2021], an adversarially trained model with a small maximum  $L_2$  norm perturbation  $\varepsilon$  of 0.1 and with the PGD attack applied with 3 steps and a step size equal to  $2\varepsilon/3$ . On CIFAR-10, we reuse the best hyperparameters of Springer et al. [2021] to adversarially train the SAT surrogate model with a maximum  $L_2$  norm  $\varepsilon$  of 0.025 and PGD with 7 steps and a step size of  $0.3\varepsilon$ . For a fair comparison, we choose the best checkpoint of the early stopped SGD surrogate by evaluating the transferability of every training epoch. For each epoch, we craft 1,000 adversarial examples from a distinct validation set of original examples and compute their success rate over a distinct set of validation target architectures. On CIFAR-10, the selected epoch is 54, and 66 on ImageNet. All the other hyperparameters not mentioned in this paragraph are the same as those used to train the surrogates with SGD.

**Non-surrogate training transferability techniques (Section 6).** We consider nine transferability techniques that are not surrogate training techniques, i.e., model augmentation (GN, SGM, LGV), data augmentation (DI, SI, VT), attack optimizers (MI, NI, RAP). We study their complementarity with our surrogate training technique. SI uses  $m = 5$  copies. VT uses  $\beta = 1.8$ . GN uses a random range of  $[1 - 0.3, 1 + 0.3]$ . We use the following hyperparameters. MI uses a decay of 1.2 and NI a decay of 0.6. DI uses a resize rate of 0.85 with a diversity probability of 0.8. We apply the inner optimization of RAP (gradient ascent) with 5 steps and a search neighborhood  $\varepsilon_n = \frac{2}{3}\varepsilon$  to keep the original proportion. Our preliminary experiments confirm the observation of Qin et al. [2022] that starting the inner optimization from the first outer optimization step is not optimal. For fairness to RAP, we start the inner optimization at the 10th step of the outer optimization.

**Attack.** Unless specified otherwise, we use the BIM (Basic Iterative Method, equivalently called I-FGSM) Kurakin et al. [2017] which is the standard attack for transferability Benz et al. [2021], Dong et al. [2018], Gubri et al. [2022a,b], Li et al. [2018], Lin et al. [2019], Springer et al. [2021], Wu et al. [2020], Xie et al. [2019], Zhao et al. [2022], Qin et al. [2022]. By default, the maximum  $L_\infty$  perturbation norm  $\varepsilon$  is set to  $4/255$ . We use the BIM hyperparameters tuned by Gubri et al. [2022a,b] on a distinct set of validation target models: BIM performs 50 iterations with a step size equal to  $\varepsilon/10$ . Unless specified otherwise, we craft adversarial examples from a subset of 1,000 natural test examples that are correctly predicted by all target models. We repeat the experiments on CIFAR-10 three times, each run with a different random seed, an independently sampled subset of original examples, and *an independently trained surrogate model*. For every CIFAR-10 experiment, we train three times each surrogate model to estimate correctly the randomness of an attacker training a surrogate model to perform an attack. The success rate is the misclassification rate of these adversarial examples evaluated on one target model. We report the average success rate across the three random seeds, along with a confidence interval of plus/minus two times the empirical standard deviation.

**Threat model.** We study the threat model of untargeted adversarial examples: the adversary’s goal is misclassification. We consider the standard adversary capability for transfer-based black-box attacks, where the adversary does not have query access to the target model. Query-based attacks are another distinct family of attacks. The attacker does not know the weights of the target model, nor its architecture. Similarly to all the related work [Benz et al., 2021, Dong et al., 2018, Gubri et al., 2022a,b, Li et al., 2018, Lin et al., 2019, Springer et al., 2021, Wu et al., 2020, Xie et al., 2019, Zhao et al., 2022, Qin et al., 2022], we suppose that the attacker can independently train a surrogate model on the same training data.

**Sharpness metrics.** We compute both sharpness metrics (Hessian top-1 eigenvalue and Hessian trace) at every epoch using the PyHessian library [Yao et al., 2019] on a random subset of a thousand examples from the CIFAR-10 train dataset.

**Implementation.** The source code for each experiment is available on GitHub. Our models are distributed through HuggingFace. We use the torchattacks library [Kim, 2020] to craft adversarial examples with the BIM attacks and four transferability techniques, namely LGV, DI, SI, VT, MI and NI. We reuse the original implementations of GN and SGM to “patch” the surrogate architecture, and use the TorchAttacks implementation of BIM on top. We adapted the original implementation of RAP to fit our experimental settings. The software versions are the following: Python 3.10.8, PyTorch 1.12.1, Torchvision 0.13.1, and TorchAttacks 3.3.0.

**Infrastructure.** For all experiments, we use Tesla V100-DGXS-32GB GPUs on a server with 256GB of RAM, CUDA 11.4, and the Ubuntu operating system.

Table 5: Hyperparameters used to train surrogate models.

Training	Hyperparameter	Dataset	Value
All	Number of epochs	CIFAR-10	150
		ImageNet	90
	Initial learning rate	All	0.1
	Learning rate decay	CIFAR-10	Step-wise /10 each 50 epochs
		ImageNet	Step-wise /10 each 30 epochs
	Momentum	All	0.9
	Batch-size	CIFAR-10	128
		ImageNet	256
	Weight decay	CIFAR-10	0.0005
		ImageNet	0.0001
SAM	$\rho$	All	0.05 for SAM, 0.4 for l-SAM
GSAM	$\rho$	All	0.05 for GSAM, 0.2 for l-GSAM
	$\alpha$	All	0.15
LookSAM	$\rho$	All	0.05 for LookSAM, 0.3 for l-LookSAM
	$k$	All	5
	SAM Warmup	All	3 epochs
ASAM	$\rho$	All	0.5 for ASAM, 3 for l-ASAM
AGSAM	$\rho$	All	0.5 for AGSAM, 4 for l-AGSAM
	$\alpha$	All	0.15

## B TRANSFERABILITY AND NATURAL ACCURACY BY EPOCHS

Early stopping clearly benefits transferability for all ten targets on CIFAR-10 and all ten targets on ImageNet (except for the two Vision Transformers, where the transferability plateaus). We reproduce below the success rates for all target models from the ResNet-50 surrogate model on both CIFAR-10 (Figure 7) and ImageNet (Figure 9) datasets. We also report the evolution of the natural accuracy for both CIFAR-10 (Figure 8) and ImageNet (Figure 10).

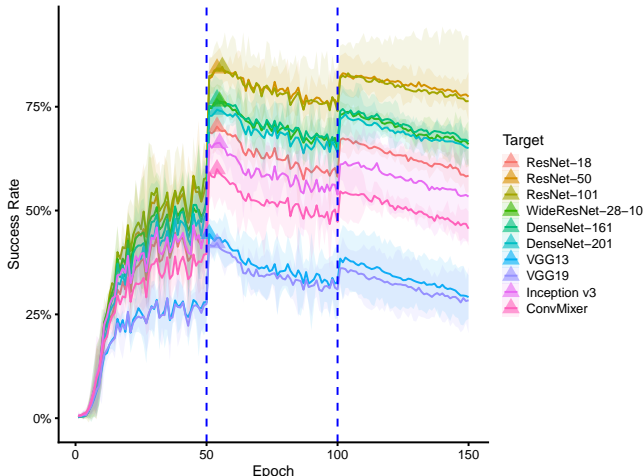


Figure 7: Early stopping improves transferability consistently across target models on CIFAR-10. Success rate evaluated on ten target models (color) from a ResNet-50 surrogate model trained for a number of epochs (x-axis) on the CIFAR-10 dataset. We report the average over three random seeds (line) and the confidence interval of two standard deviations (colored area). Vertical bars indicate the step decays of the learning rate. Triangles indicate the epochs corresponding to the highest success rate per target.

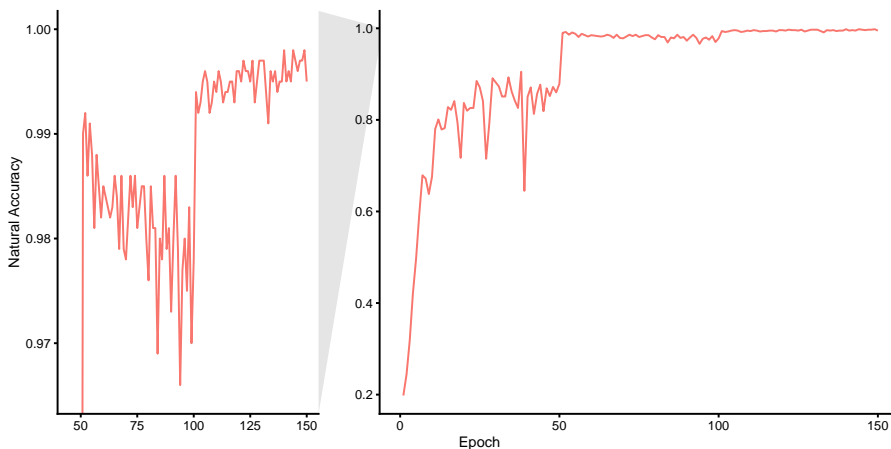


Figure 8: The natural accuracy increases at the end of training, whereas transferability decreases. Natural test accuracy of the ResNet-50 surrogate model trained for a number of epochs (x-axis) on the CIFAR-10 dataset. Evaluated on the test subset used to craft adversarial examples in Figure 7.

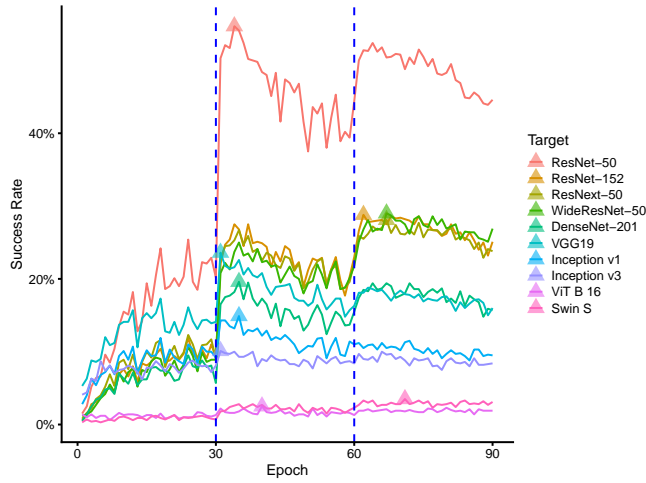


Figure 9: Early stopping improves transferability to various target models on ImageNet, except to vision transformers (ViT-B-16 and Swin-S) against which the success rate plateaus at the end of training. Success rate evaluated on ten target models (colour) from a ResNet-50 surrogate model trained for a number of epochs (x-axis) on the ImageNet dataset. Vertical bars indicate the step decays of the learning rate. Triangles indicate the epochs corresponding to the highest success rate per target.

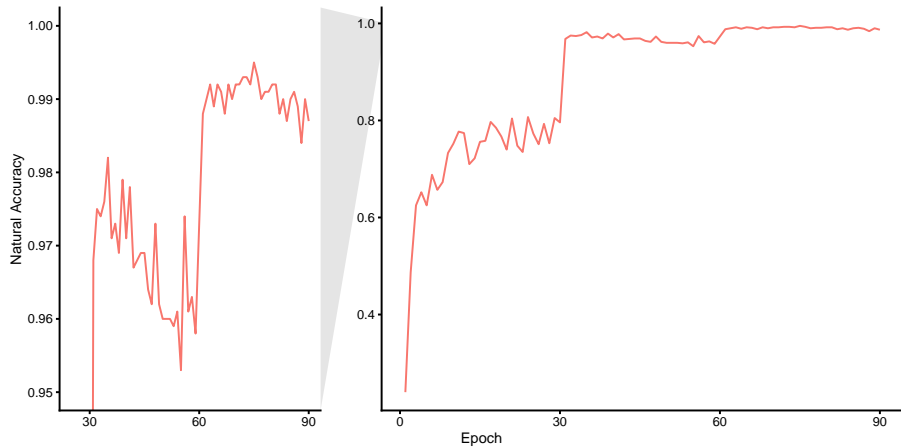


Figure 10: Natural test accuracy of the ResNet-50 surrogate model trained for a number of epochs (x-axis) on the ImageNet dataset. Evaluated on the test subset used to craft adversarial examples in Figure 9.

## C ANOTHER LOOK AT THE NON-ROBUST FEATURES HYPOTHESIS ABOUT EARLY STOPPING

This section contains detailed results of Section 3. Figure 11 reports the transferability per target of the experiment that shows the success of early stopping for surrogates trained on both robust and non-robust datasets. For this experiment, we divided by two the initial learning rate (0.05) when training on  $D_{NR}$  due to instabilities during training when trained with a learning rate of 0.1.

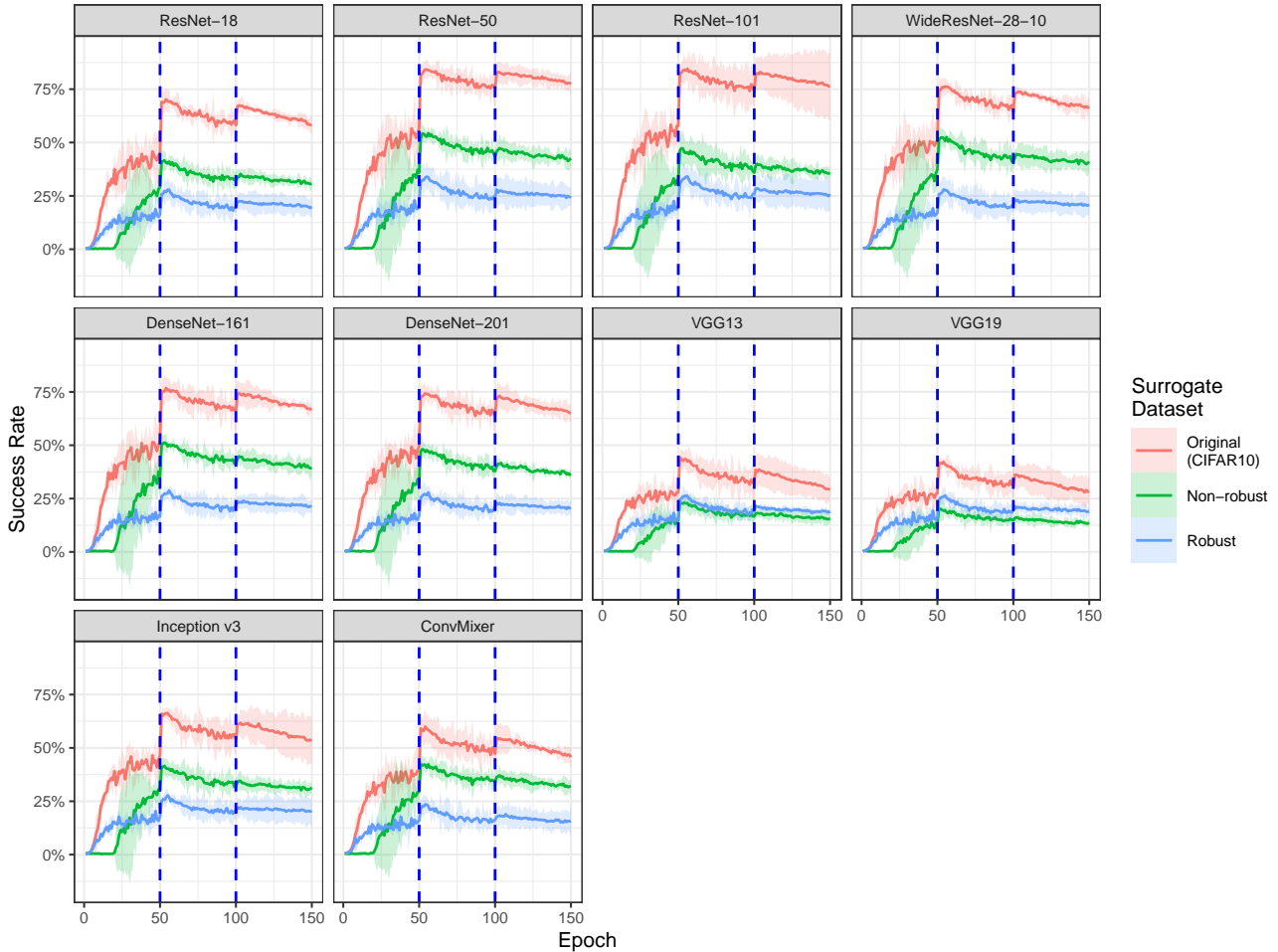


Figure 11: Early stopping improves transferability of surrogate models trained on both robust and non-robust datasets. Success rate evaluated over ten target models (title subfigure) from a ResNet-50 surrogate model trained for a number of epochs (x-axis) on the datasets  $D_R$  (blue) and  $D_{NR}$  (green) of Ilyas et al. [2019] modified from CIFAR-10 (red).

## D TRANSFERABILITY AND TRAINING DYNAMICS

This section contains additional results of Section 4 on the relationship between the training dynamics of the surrogate model and its transferability.

### D.1 CONSISTENCY OF THE PEAK OF TRANSFERABILITY

Figure 12 contains the transferability per target of the surrogate models trained with a single learning rate decay at a varying epoch. The consistency of the peak of transferability across training epochs is valid for all ten targets.

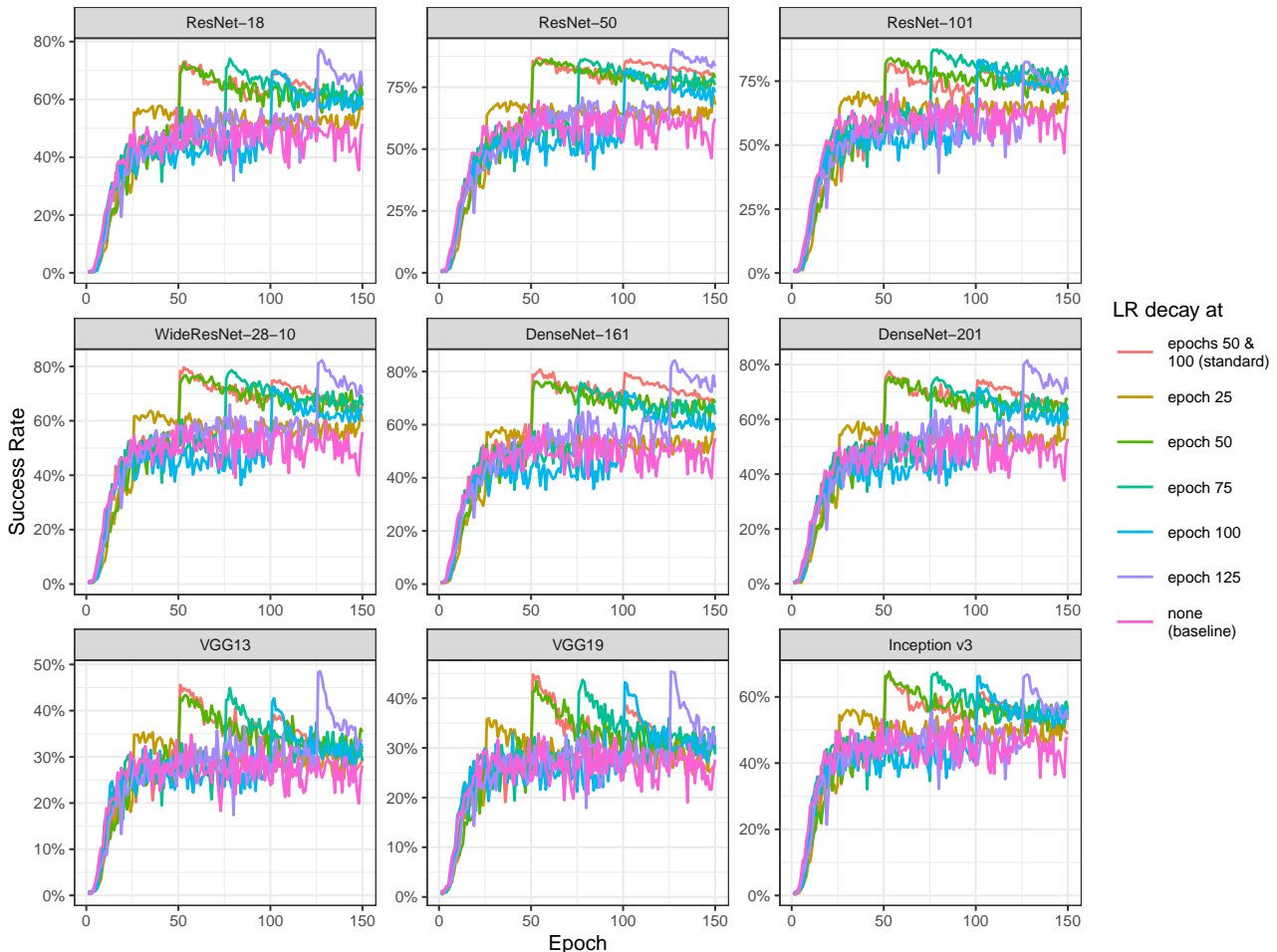


Figure 12: Step learning rate decay benefits transferability at any epochs. Success rate evaluated over nine target models (title subfigure) from a ResNet-50 surrogate model trained for a number of epochs (x-axis) on the CIFAR-10. The LR is divided by 10 a single time during training at an epoch indicated by the color. Scale not shared between subfigures.

### D.2 CROSSING THE VALLEY BEFORE EXPLORING THE VALLEY

Before the learning rate decays, the exploration tends to behave more like “crossing the valley” than after decay, when it is more likely to “crawl down to the valley”, as described in Schneider et al. [2021]. Figure 1 illustrates this phenomenon. Schneider et al. [2021] proposes the  $\alpha$ -quantity, a metric computed at the level of SGD iterations to disentangle whether the iteration understeps or overshoots the minimum along the current step direction. Based on a noise-informed quadratic fit,  $\alpha \approx 0$  indicates an appropriate LR that minimizes the loss in the direction of the gradient at this iteration (“going down to the valley”).  $\alpha > 0$  indicates that the current LR overshoots this minimum (“crossing the valley”). We compute the

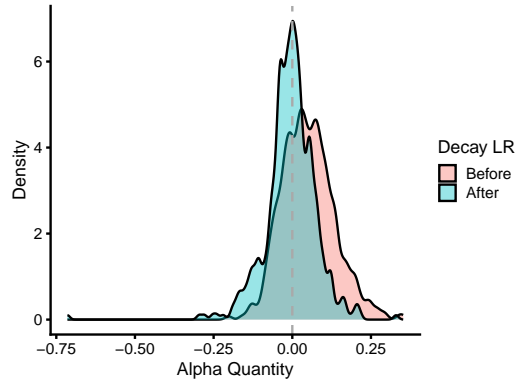


Figure 13: The LR decay corresponds to a transition from a “crossing the valley” phase to a “crawling down to the valley” phase. Density plot of the  $\alpha$ -quantity values computed each four SGD iterations during the best five epochs for transferability on CIFAR-10 (epochs 50–54, “After” group, blue) and the five preceding epochs (epochs 45–49, “Before” group, red).

$\alpha$ -quantity every four SGD iterations during the best five epochs for transferability on CIFAR-10 (“after LR decay”, epochs 50–54) and during the five preceding epochs (“before LR decay”, epochs 45–49). The one-sided Welch Two Sample t-test has a p-value inferior to  $2.2e^{-16}$ . We reject the null hypothesis in favor of the alternative hypothesis that the true difference of  $\alpha$ -quantity in means between the group “before LR decay” and the group “after LR decay” is strictly greater than 0. We also perform a one-sided Welch Two Sample t-test on the 5 epochs before and after the second LR decay (epochs 95–99 vs. epochs 100–105). Its p-value is equal to 0.004387. Using the Bonferroni correction, we compare the p-values of both individual tests with a significance threshold of 0.5%. We reject the null hypothesis for both LR decays with a significance level of 1%. Figure 13 is the density plot of the  $\alpha$ -quantities for both groups. Our results suggest that before the LR decay, training is slow due to a “crossing the valley” pattern. The best early stopped surrogate occurs a few training epochs after the LR decay when the SGD starts exploring the bottom of the valley.

## E TRANSFERABILITY FROM SAM AND ITS VARIANTS

This section presents the following elements:

1. A description of SAM and its variants (Section E.1),
2. The success rate with respect to the  $\rho$  hyperparameter of SAM and its variants, used to tune this hyperparameter for transferability (Section E.2),
3. The natural accuracy of the surrogates trained by SAM and its variants (Section E.3).

### E.1 DESCRIPTION OF SAM AND ITS VARIANTS

This section describes SAM and its variants. It includes an illustrative schema of SAM (Figure 14).

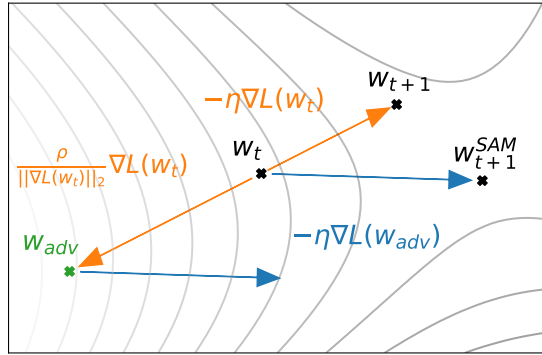


Figure 14: Illustrative schema of a training iteration with SAM. Illustration from Foret et al. [2020].

**SAM** SAM [Foret et al., 2020] minimizes the maximum loss around a neighborhood by performing a gradient ascent step.

First, the gradient ascent step is performed (left orange in Figure 14) to compute  $\epsilon_t = \rho \frac{\nabla \mathcal{L}(w_t)}{\|\nabla \mathcal{L}(w_t)\|_2}$ . It is followed by a gradient descent step,  $w_{t+1} = w_t - \alpha_t (\nabla \mathcal{L}(w_t + \epsilon_t) + \lambda w_t)$  (blue arrows in Figure 14).

**LookSAM** LookSAM [Liu et al., 2022] is an efficient alternative that computes only the additional ascending gradient of SAM once per five training iterations, i.e.,  $\epsilon_t = \epsilon_{\lfloor \frac{t}{5} \rfloor}$ . We faced some convergence issues when applying it with our learning rate schedule (the original authors used a schedule with warmup). To solve this issue, we add some warmup: LookSAM computes both gradients for the first three epochs of training, exactly as SAM. From the fourth epoch, the training resumes to the efficient LookSAM variant. The computational cost reported in Table 3 takes into account this overhead.

**ASAM** ASAM [Kwon et al., 2021] is an adaptive variant of SAM. ASAM introduces a normalization operator  $T_w^{-1}$  to adjust the maximization region with respect to the weight scale. The maximization step becomes:  $\epsilon_t = \rho \frac{T_{w_t}^2 \nabla \mathcal{L}_s(w_t)}{\|T_{w_t} \nabla \mathcal{L}_s(w_t)\|_2}$ . We follow the original paper Kwon et al. [2021] to select the hyperparameter  $\rho$ : the authors recommend multiplying  $\rho$  by 10 when switching to an adaptive variant.

**GSAM** GSAM [Zhuang et al., 2022] introduces a decomposition of the gradient computed in the maximization step. Only the orthogonal component is then used in the minimization step. AGSAM is the combination of GSAM and ASAM.

### E.2 THE SIZE OF FLAT NEIGHBORHOODS: THE CHOICE OF THE $\rho$ HYPERPARAMETER

A stronger regularization induced by SAM with large flat neighborhoods trains a better surrogate model. The size of flat neighborhoods is controlled by the unique hyperparameter of SAM, noted  $\rho$ . Figure 15 reports the validation success rate used to find the best large  $\rho$  for each SAM variants. The selected  $\rho$  values are reported for each SAM variant in Table 5. This success rate is computed on a separate set of target models, surrogate models, and a set of examples. This experimental setting is carefully designed to avoid data leakage by optimizing the hyperparameter against specific target

models. Otherwise, this could result in model selection, similar to query-based attacks, which are not allowed by our threat model of transfer-based black-box attacks.

Figure 16 reports the test success rate on the same surrogate models, but computed on our test set of target models and using natural examples from the test set. Sections 5 and 6 report results from three other independently trained surrogate models. The transferability improvement of LookSAM with large  $\rho$  is tiny compared to LookSAM with the original  $\rho$ . LookSAM is an efficient variant of SAM that skips 4/5 of the additional ascending gradients of SAM. Our hypothesis is that training with large  $\rho$  requires a more refined update strategy.

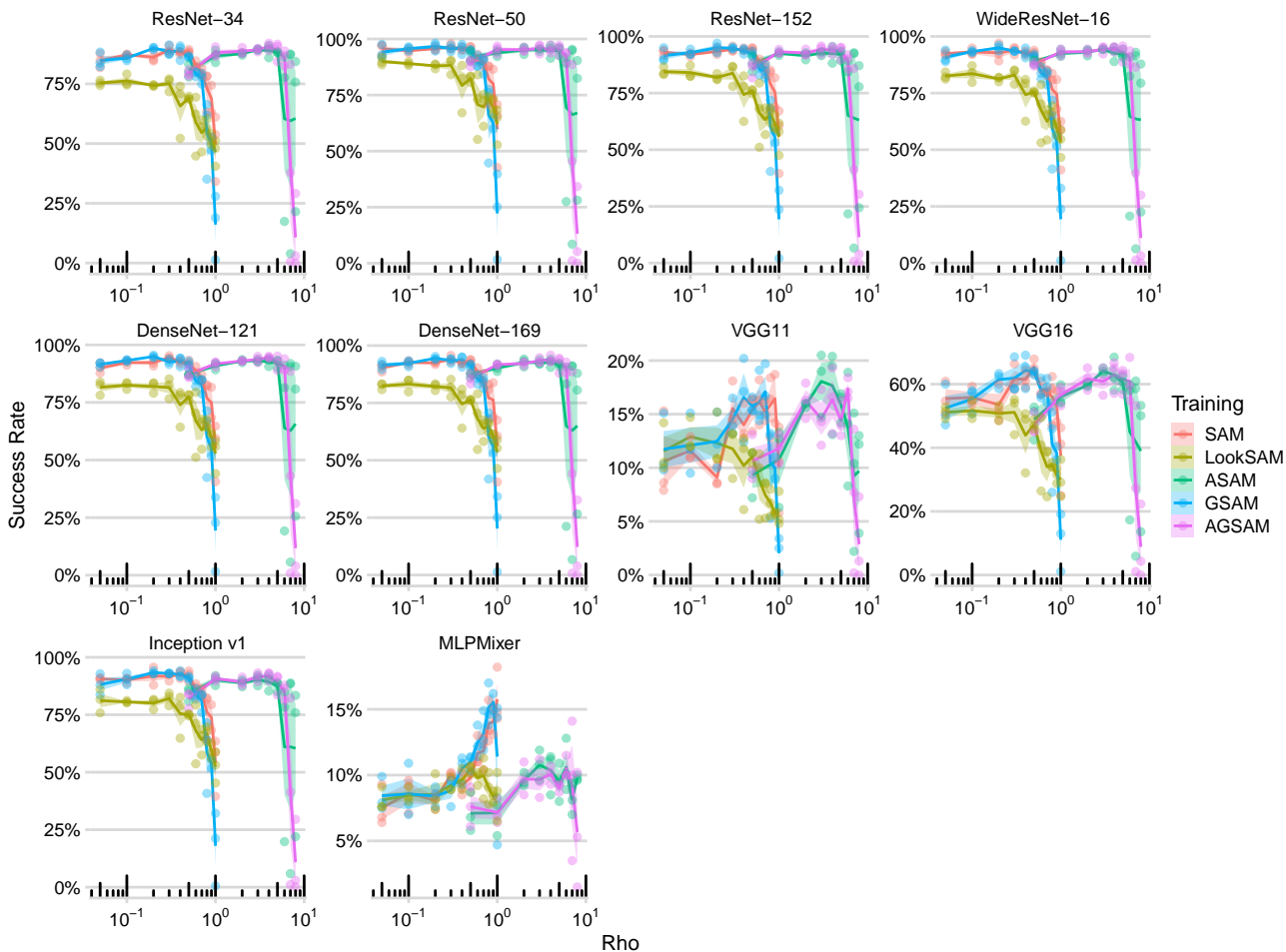


Figure 15: All SAM variants trains better surrogate models with a larger  $\rho$  than the original one, used for natural accuracy. *Validation* success rate on ten validation target models (subfigure title) from a ResNet-50 surrogate model trained using SAM or SAM variants (colors) with various  $\rho$  hyperparameters (x-axis) on the CIFAR-10 dataset. Adversarial examples are crafted from a disjoint subset of one thousand original examples from the train set. The left most  $\rho$  value is the original one: 0.5 for adaptive variants (ASAM, AGSAM), 0.05 for others. Average (line) and  $\pm$  one standard deviation (colored area) of three training runs.

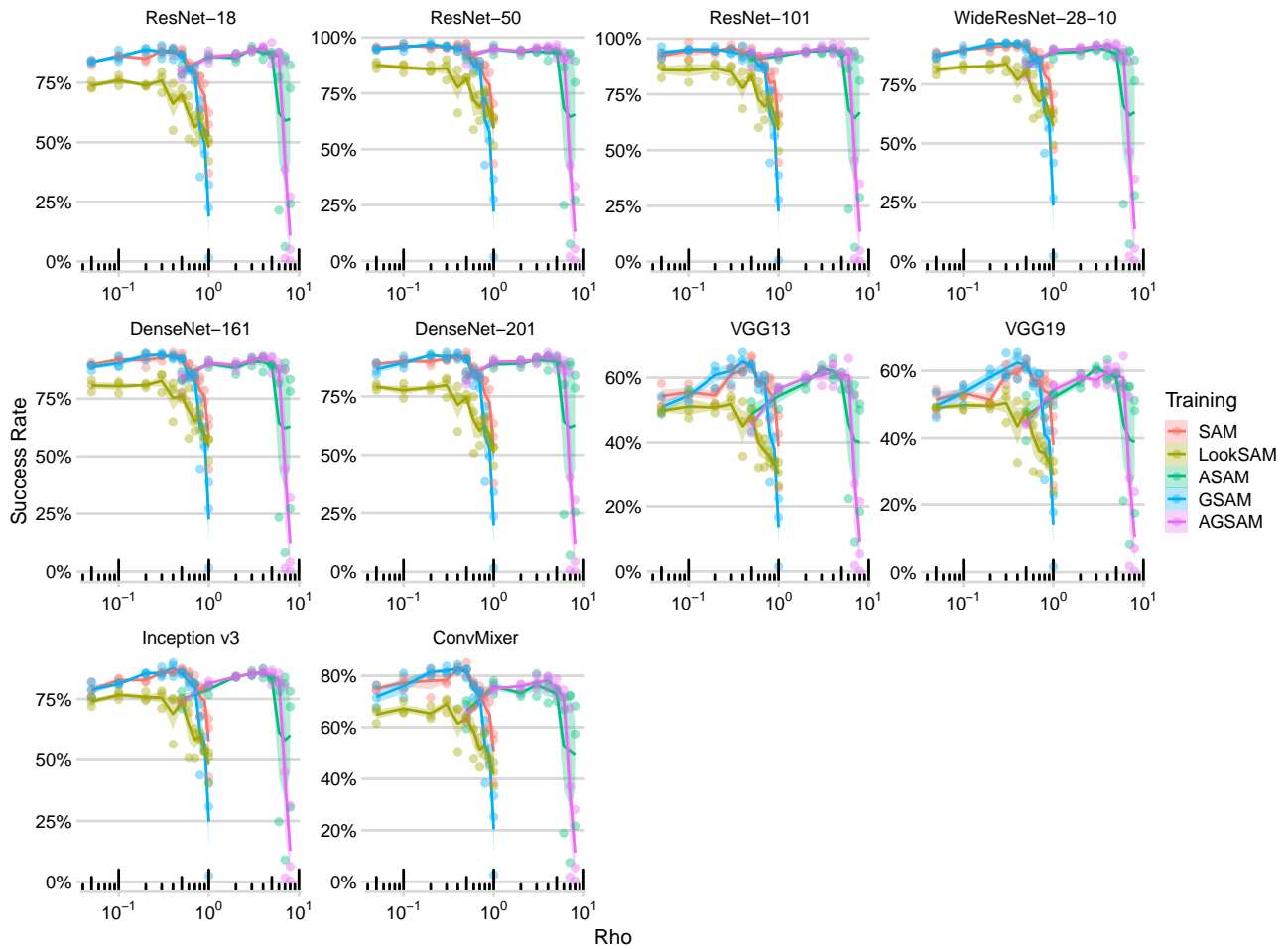


Figure 16: All SAM variants trains better surrogate models with a larger  $\rho$  than the original one, used for natural accuracy. *Test* success rate on ten test target models (subfigure title) from a ResNet-50 surrogate model trained using SAM or SAM variants (colors) with various  $\rho$  hyperparameters (x-axis) on the CIFAR-10 dataset. Adversarial examples are crafted from a disjoint subset of one thousand original examples from the test set. The left most  $\rho$  value is the original one: 0.5 for adaptive variants (ASAM, AGSAM), 0.05 for others. Average (line) and  $\pm$  one standard deviation (colored area) of three training runs. The surrogate models used here are the same as in Figure 15. Nevertheless, Sections 5 and 6 report results from three other independently trained surrogate models.

### E.3 NATURAL ACCURACY OF SAM AND ITS VARIANTS

Tables 6 and 7 report the natural test accuracies of the surrogate models studied in Sections 5 and 6. As commented in Section 5, the strong regularization induced by SAM with large flat neighborhoods (high  $\rho$ ) can degrade natural generalization. In particular, on ImageNet, our ResNet-18 and ResNet-50 surrogates trained with l-SAM have a worst natural accuracy compared to SAM and even fully trained SGD. On CIFAR-10, l-SAM has an inferior natural accuracy than SAM, and a similar one to SGD. Therefore, the improvement in transferability from l-SAM, i.e., *the generalization of adversarial examples from this strong regularization, cannot be explained by an improvement in natural generalization*, i.e, a better fit to the data.

Table 6: Accuracy computed on the test set of the surrogates trained by SAM and its variants on ImageNet. In %.

Arch	Training	Size neighborhood	Accuracy
ResNet-18	SGD (baseline)	None (SGD)	69.8
ResNet-18	SAM	Large	67.9
ResNet-18	SAM	Original	70.3
ResNet-18	GSAM	Large	68.8
ResNet-18	GSAM	Original	70.3
ResNet-18	ASAM	Large	68.9
ResNet-18	ASAM	Original	70.2
ResNet-18	AGSAM	Large	67.8
ResNet-18	AGSAM	Original	70.1
ResNet-50	SGD (baseline)	None (SGD)	75.7
ResNet-50	SAM	Large	74.5

Table 7: Accuracy computed on the test set of the surrogates trained by SAM and its variants on CIFAR-10. In %.

Arch	Training	Size neighborhood	Accuracy
ResNet-50	SGD (baseline)	None (SGD)	94.5 $\pm$ 0.4
ResNet-50	SAM	Large	94.6 $\pm$ 0.4
ResNet-50	SAM	Original	95.3 $\pm$ 0.3
ResNet-50	GSAM	Large	94.7 $\pm$ 0.5
ResNet-50	GSAM	Original	95.4 $\pm$ 0.5
ResNet-50	ASAM	Large	95.6 $\pm$ 0.5
ResNet-50	ASAM	Original	95.1 $\pm$ 0.4
ResNet-50	AGSAM	Large	95.9 $\pm$ 0.3
ResNet-50	AGSAM	Original	95.3 $\pm$ 0.6

## F TRANSFERABILITY AND WEIGHT DECAY

We show that in the case of weight decay, a stronger regularization of the surrogate model does not improve transferability. Unlike weight decay, the stronger regularization of SAM is tightly linked to transferability.

We train on CIFAR-10 one surrogate model for various values of the weight decay regularization ( $5e-3$ ,  $1e-3$ ,  $5e-4$ ,  $1e-4$ ,  $5e-5$ ,  $1e-5$  and  $5e-6$ ) and for various capacities of the ResNet architecture (ResNet-18, ResNet-50, ResNet-101). Figure 17 presents the transferability of these surrogates. For the ResNet-50 and ResNet-101 surrogates, the best average success rate simply corresponds to the weight decay used to train the target models. Interestingly, a lighter weight decay regularization trains better ResNet-18 surrogate models. We hypothesize that a higher regularization allows this smaller architecture to better mimic the complexities of the larger architectures used as targets. Overall, a stronger weight decay regularization does not train better surrogate models, contrary to the SAM regularization.

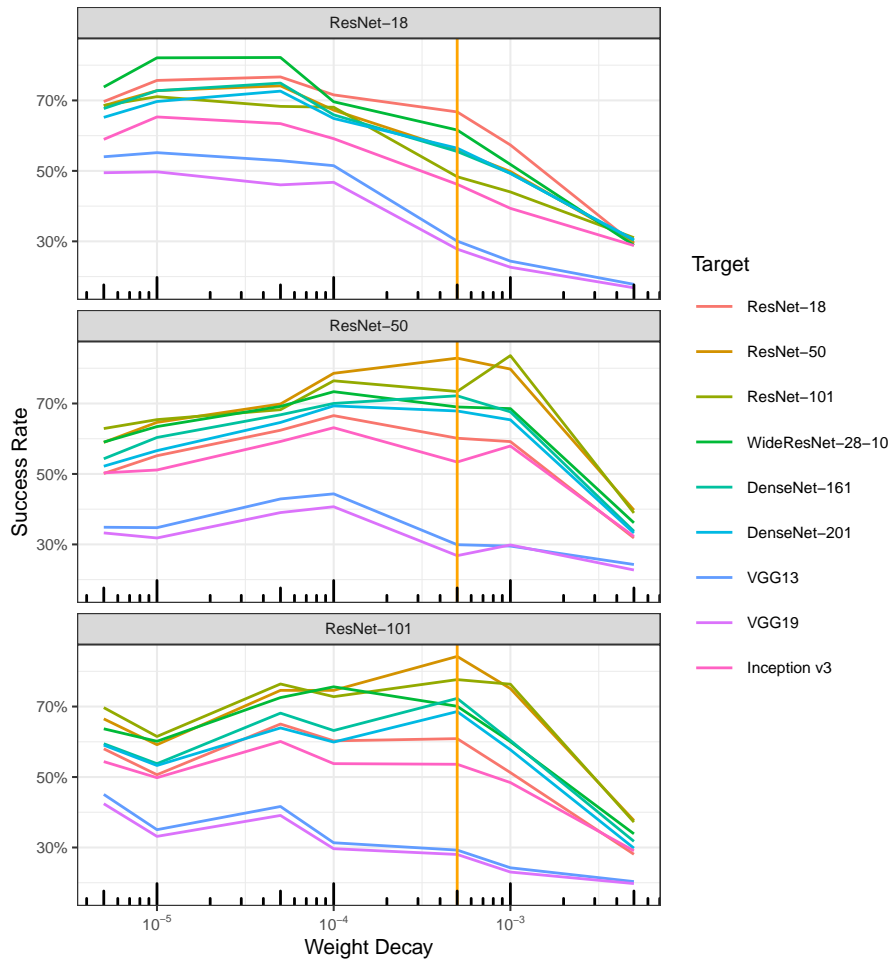


Figure 17: Stronger weight decay regularization does not improve transferability. Success rate from ResNet surrogates (subfigure title) trained with a weight decay (x-axis) evaluated on targets (colors) trained with weight decay indicated by the yellow vertical bar on the CIFAR-10 dataset.

## G EVALUATION OF L-SAM: IMPROVING TRANSFERABILITY TECHNIQUES WITH SHARPNESS MINIMIZATION

This section extends the evaluation of SAM with large flat neighborhoods of Section 6, performed with  $\varepsilon$  equal to  $4/255$ , to two other perturbation  $L_\infty$  norms ( $2/255$  and  $8/255$ ) for the competitive techniques, and reports the success rate per target for the complementary techniques.

**Evaluation against competitive techniques.** Tables 8 and 10 evaluate competitive techniques of l-SAM on CIFAR-10 with, respectively, maximum perturbations  $L_\infty$  norm  $\varepsilon$  of  $2/255$  and  $8/255$ . The same conclusions made with perturbations of size  $4/255$  hold for these two norms: l-SAM clearly improves transferability. l-SAM beats other competitive techniques for the ten targets and both norms. Tables 11, 12, and 13 show, respectively, that l-SAM beats the other techniques in 6 out of 10 targets for  $\varepsilon$  equal to  $2/255$ , and in 5 out of 10 targets for  $\varepsilon$  equal to  $8/255$ .

**Evaluation with complementary techniques.** Tables 14, 15, and 16 report in detail per target the evaluation of complementary transferability techniques on ImageNet. l-SAM increases the transferability of every nine techniques against every ten targets when combined, except for LGV on 4 targets using  $\varepsilon$  equals  $2/255$ , and LGV on 3 targets with  $\varepsilon$  equals  $4/255$  or  $8/255$ . Since LGV collects models with SGD and a high learning rate, a conflict might occur when LGV continues training with SGD from a checkpoint trained with SAM. Future work may explore the adaptation of the LGV model collection to SAM.

Table 8: Success rate on CIFAR-10 of competitive techniques to train a single surrogate model. Adversarial examples evaluated on nine targets with a maximum perturbation  $L_\infty$  norm  $\varepsilon$  of  $2/255$ . Bold is best. In %.

Surrogate	Target								
	RN18	RN50	RN101	DN161	DN201	VGG13	VGG19	IncV3	WRN28
Fully Trained SGD	24.2	44.7	35.6	33.3	31.4	9.6	9.2	22.6	30.8
Early Stopped SGD	28.6	46.1	38.6	36.3	34.6	12.7	13.0	27.1	34.9
SAT	19.7	27.3	25.4	20.1	20.3	13.4	13.5	17.6	20.5
l-SAM (ours)	<b>45.4</b>	<b>67.1</b>	<b>60.6</b>	<b>58.9</b>	<b>55.8</b>	<b>20.5</b>	<b>19.8</b>	<b>45.0</b>	<b>54.1</b>

Table 9: Success rate on CIFAR-10 of competitive techniques to train a single surrogate model. Adversarial examples evaluated on nine targets with a maximum perturbation  $L_\infty$  norm  $\varepsilon$  of  $4/255$ . Bold is best. In %.

Surrogate	Target								
	RN18	RN50	RN101	DN161	DN201	VGG13	VGG19	IncV3	WRN28
Fully Trained SGD	57.9	81.2	70.6	70.8	66.1	27.8	26.3	49.4	66.5
Early Stopped SGD	73.3	87.8	82.1	81.4	78.3	45.5	44.3	66.8	79.5
SAT	66.3	76.2	73.6	66.9	66.1	49.8	48.5	57.9	67.8
l-SAM (ours)	<b>89.7</b>	<b>97.3</b>	<b>95.5</b>	<b>95.7</b>	<b>94.0</b>	<b>63.6</b>	<b>60.6</b>	<b>87.3</b>	<b>93.0</b>

Table 10: Success rate on CIFAR-10 of competitive techniques to train a single surrogate model. Adversarial examples evaluated on nine targets with a maximum perturbation  $L_\infty$  norm  $\varepsilon$  of  $8/255$ . Bold is best. In %.

Surrogate	Target								
	RN18	RN50	RN101	DN161	DN201	VGG13	VGG19	IncV3	WRN28
Fully Trained SGD	88.3	97.4	92.4	93.9	91.4	64.2	60.5	79.3	91.9
Early Stopped SGD	97.8	99.6	98.8	98.9	98.4	89.1	87.5	95.6	98.8
SAT	97.0	98.7	98.0	97.1	96.4	90.2	89.2	93.2	97.1
l-SAM (ours)	<b>99.7</b>	<b>100.0</b>	<b>100.0</b>	<b>100.0</b>	<b>99.9</b>	<b>96.6</b>	<b>95.6</b>	<b>99.6</b>	<b>99.9</b>

Table 11: Success rate on ImageNet of competitive techniques to train a single surrogate model. Adversarial examples evaluated on ten targets with a maximum perturbation  $L_\infty$  norm  $\varepsilon$  of  $2/255$ . Bold is best. In %.

Surrogate	Target									
	RN50	RN152	RNX50	WRN50	VGG19	DN201	IncV1	IncV3	ViT B	SwinS
Fully Trained SGD	18.7	9.4	10.0	9.3	7.6	5.8	4.8	5.2	1.1	1.4
Early Stopped SGD	23.8	10.7	10.6	10.6	8.7	6.8	5.6	6.1	1.1	1.5
LGV-SWA	49.3	24.8	25.0	21.7	18.5	16.8	11.6	7.9	1.4	1.5
SAT	30.0	19.2	24.4	20.6	18.4	20.2	<b>20.0</b>	<b>16.6</b>	<b>4.9</b>	<b>4.4</b>
l-SAM (ours)	<b>53.3</b>	<b>34.3</b>	<b>37.5</b>	<b>38.3</b>	<b>30.7</b>	<b>25.0</b>	16.6	10.8	1.7	3.8

Table 12: Success rate on ImageNet of competitive techniques to train a single surrogate model. Adversarial examples evaluated on ten targets with a maximum perturbation  $L_\infty$  norm  $\varepsilon$  of  $4/255$ . Bold is best. In %.

Surrogate	Target									
	RN50	RN152	RNX50	WRN50	VGG19	DN201	IncV1	IncV3	ViT B	SwinS
Fully Trained SGD	44.5	25.2	24.8	27.1	16.2	16.4	9.8	8.0	1.8	3.3
Early Stopped SGD	51.5	27.4	27.7	28.0	18.4	18.7	10.8	10.4	2.2	2.7
LGV-SWA	82.5	56.8	58.5	54.0	40.9	42.4	28.3	15.1	3.1	5.7
SAT	76.3	62.5	66.8	63.4	48.1	<b>59.0</b>	<b>47.9</b>	<b>40.8</b>	<b>17.4</b>	<b>16.8</b>
l-SAM (ours)	<b>85.7</b>	<b>70.3</b>	<b>73.3</b>	<b>73.2</b>	<b>58.2</b>	55.6	37.9	20.5	4.0	8.2

Table 13: Success rate on ImageNet of competitive techniques to train a single surrogate model. Adversarial examples evaluated on ten targets with a maximum perturbation  $L_\infty$  norm  $\varepsilon$  of  $8/255$ . Bold is best. In %.

Surrogate	Target									
	RN50	RN152	RNX50	WRN50	VGG19	DN201	IncV1	IncV3	ViT B	SwinS
Fully Trained SGD	77.5	52.9	51.1	55.0	33.4	36.9	21.1	15.2	3.7	6.7
Early Stopped SGD	82.0	56.8	54.6	59.2	35.9	41.1	24.8	18.3	3.6	5.9
LGV-SWA	96.9	87.7	87.1	84.9	65.4	72.8	56.8	31.2	7.0	12.3
SAT	95.4	92.6	93.0	92.8	79.0	<b>90.1</b>	<b>79.1</b>	<b>66.3</b>	<b>38.5</b>	<b>39.1</b>
l-SAM (ours)	<b>97.6</b>	<b>92.8</b>	<b>93.8</b>	<b>95.3</b>	<b>83.2</b>	85.5	71.2	42.3	9.1	19.0

Table 14: Success rate on ImageNet of three complementary categories of transferability techniques evaluated on ten targets with a maximum perturbation  $L_\infty$  norm  $\varepsilon$  of  $2/255$ . Underlined is worse when combined with l-SAM. In %.

Attack	Target									
	RN50	RN152	RNX50	WRN50	VGG19	DN201	IncV1	IncV3	ViT B	SwinS
<b>Model Augmentation Techniques</b>										
GN	34.6	17.9	17.4	18.0	12.7	10.4	8.1	6.3	1.3	2.0
GN + l-SAM	59.7	42.2	42.8	45.4	35.4	29.1	18.3	11.0	1.8	2.4
SGM	26.9	14.9	15.2	15.8	15.5	9.7	7.4	6.6	1.6	3.6
SGM + l-SAM	46.3	32.0	33.8	35.5	33.4	21.8	20.3	11.9	2.7	5.6
LGV	59.8	33.0	32.9	28.4	31.1	24.2	21.3	12.5	2.4	2.6
LGV + l-SAM	<u>50.7</u>	<u>31.3</u>	32.9	31.4	33.5	27.9	25.0	14.3	<u>2.1</u>	<u>2.5</u>
<b>Data Augmentation Techniques</b>										
DI	46.1	27.2	30.9	30.3	22.4	24.8	17.8	15.0	2.5	4.1
DI + l-SAM	66.6	49.5	57.1	52.3	54.1	49.3	47.5	31.8	4.4	6.9
SI	26.2	14.2	14.3	13.3	10.4	11.3	8.4	7.3	0.9	1.4
SI + l-SAM	56.5	37.9	42.9	41.2	33.0	31.4	25.0	14.7	2.1	2.9
VT	26.5	14.4	14.1	13.6	10.8	10.1	6.1	6.3	1.3	2.2
VT + l-SAM	61.5	43.0	47.0	47.4	39.4	35.9	24.3	13.3	2.1	4.9
<b>Attack Optimizers</b>										
MI	29.8	15.9	16.4	16.2	12.6	11.5	7.7	8.0	1.9	2.7
MI + l-SAM	58.2	41.5	45.4	44.6	39.8	35.8	28.9	17.4	2.8	5.4
NI	21.1	11.0	10.9	11.2	8.4	6.9	5.0	5.2	1.3	1.7
NI + l-SAM	44.1	28.5	30.7	32.0	25.9	19.6	11.9	9.1	1.3	2.4
RAP	27.6	15.1	15.5	14.4	12.1	10.4	7.5	7.8	1.7	2.6
RAP + l-SAM	54.5	38.2	42.3	41.2	37.8	33.3	27.1	16.2	3.5	6.7

Table 15: Success rate on ImageNet of three complementary categories of transferability techniques evaluated on ten targets with a maximum perturbation  $L_\infty$  norm  $\varepsilon$  of  $4/255$ . Underlined is worse when combined with I-SAM. In %.

Attack	Target									
	RN50	RN152	RNX50	WRN50	VGG19	DN201	IncV1	IncV3	ViT B	SwinS
<b>Model Augmentation Techniques</b>										
GN	68.0	43.1	41.3	44.1	24.8	27.2	14.3	9.9	1.9	3.8
GN + I-SAM	89.6	76.6	79.4	79.9	65.7	60.3	42.2	22.4	3.8	7.8
SGM	62.8	40.6	41.5	43.5	31.9	28.0	19.3	13.2	4.1	7.9
SGM + I-SAM	83.2	68.7	71.5	73.0	67.0	56.2	48.9	26.6	6.2	13.6
LGV	93.3	78.1	75.3	73.1	64.4	61.6	49.3	28.8	5.0	6.5
LGV + I-SAM	<u>88.7</u>	<u>74.3</u>	75.7	75.7	70.3	61.9	56.8	31.5	<u>4.5</u>	7.3
<b>Data Augmentation Techniques</b>										
DI	83.1	60.5	68.1	67.3	45.4	57.9	41.4	30.7	5.7	9.9
DI + I-SAM	95.0	89.7	90.7	91.6	85.3	87.8	87.5	64.2	14.2	19.0
SI	60.0	37.9	37.3	40.0	23.9	30.0	19.6	13.5	2.6	3.8
SI + I-SAM	89.2	76.6	80.1	79.1	65.2	69.8	58.0	35.8	5.0	8.5
VT	58.6	35.0	35.2	38.5	23.9	24.7	14.9	11.0	2.3	4.9
VT + I-SAM	92.0	81.2	82.4	82.9	72.3	72.3	56.7	33.6	7.0	13.5
<b>Attack Optimizers</b>										
MI	56.8	37.4	37.5	38.9	27.0	29.3	18.4	14.6	3.5	4.8
MI + I-SAM	89.4	79.3	80.4	80.8	71.5	71.1	60.1	39.3	8.5	15.2
NI	53.7	33.1	32.9	35.1	20.5	20.8	12.2	9.4	1.8	3.9
NI + I-SAM	83.9	67.3	69.8	71.4	56.1	52.5	35.6	17.6	3.8	7.0
RAP	58.1	36.9	36.3	39.9	26.0	27.0	15.9	13.3	3.0	5.7
RAP + I-SAM	86.0	74.5	75.4	75.5	68.7	66.5	54.7	35.6	7.9	17.1

Table 16: Success rate on ImageNet of three complementary categories of transferability techniques evaluated on ten targets with a maximum perturbation  $L_\infty$  norm  $\varepsilon$  of  $8/255$ . Underlined is worse when combined with l-SAM. In %.

Attack	Target									
	RN50	RN152	RNX50	WRN50	VGG19	DN201	IncV1	IncV3	ViT B	SwinS
<b>Model Augmentation Techniques</b>										
GN	92.0	73.3	69.7	74.5	45.8	50.4	29.8	19.2	3.2	7.1
GN + l-SAM	98.2	96.5	96.5	97.4	87.3	88.3	74.4	42.9	9.0	19.4
SGM	91.2	78.4	76.2	79.2	65.1	59.7	48.2	29.1	8.9	19.6
SGM + l-SAM	97.3	95.1	96.4	96.5	91.5	88.7	84.8	59.8	18.9	32.8
LGV	99.6	97.4	95.9	95.7	87.7	91.7	79.9	47.9	8.9	16.4
LGV + l-SAM	<u>99.0</u>	<u>96.5</u>	96.2	96.7	90.7	<u>91.0</u>	85.7	53.8	9.5	17.7
<b>Data Augmentation Techniques</b>										
DI	96.1	90.7	91.8	91.4	74.1	88.1	72.4	55.0	14.2	20.4
DI + l-SAM	99.8	99.6	99.5	99.7	98.6	99.3	98.4	90.4	34.7	48.7
SI	90.4	70.0	69.9	71.9	47.8	60.2	42.6	29.3	6.5	10.3
SI + l-SAM	98.9	97.3	97.3	98.0	89.9	94.8	90.1	67.2	15.0	23.6
VT	79.6	62.8	61.1	63.5	41.9	48.4	32.2	23.3	6.3	10.5
VT + l-SAM	98.0	96.7	96.1	97.3	92.9	93.1	87.1	64.2	20.0	39.2
<b>Attack Optimizers</b>										
MI	83.3	60.9	63.3	64.3	48.7	53.8	39.2	30.4	7.4	11.7
MI + l-SAM	98.5	96.3	96.7	97.1	91.9	92.7	88.1	68.6	21.3	31.5
NI	86.2	65.3	65.1	70.3	43.6	47.1	28.7	19.6	4.7	8.3
NI + l-SAM	97.9	94.0	95.0	96.0	87.3	86.2	74.2	42.6	10.7	21.0
RAP	78.1	60.1	59.1	63.1	45.3	47.4	34.0	24.0	5.6	10.9
RAP + l-SAM	96.3	93.3	92.5	94.2	89.5	87.4	81.0	61.0	17.9	33.6